Terra Antartica
2001, 8(3), 177-196

TERRA ANTARTICA

Fault and Fracture Patterns in CRP-3 Core, Victoria Land Basin, Antarctica

T.J. WILSON[1*] & T.S. PAULSEN[2]

[1]Byrd Polar Research Center and Dept. of Geological Sciences, The Ohio State University, 125 South Oval Mall, Columbus, OH 43210 - USA
[2]Department of Geology, University of Wisconsin-Oshkosh, 800 Algoma Boulevard, Oshkosh, WI 54901 - USA

Received 13 June 2001; *accepted in revised form* 23 November 2001

Abstract - Cape Roberts Project (CRP) drillsites lie along the Transantarctic Mountains Front, separating the uplifted Transantarctic Mountains from the Victoria Land rift basin of the West Antarctic rift system. Complementary studies of fractures in core and in the borehole walls were undertaken in the third CRP drillhole (CRP-3). Though differing in some respects, the microfault pattern in CRP-3 core is strikingly similar to the orientations of both onshore and offshore faults mapped along the Transantarctic Mountains Front in this region. Most significantly, a north-northeast-striking normal-displacement microfault set is dominant in the core, parallel to the main fault sets mapped on Roberts Ridge and in coastal outcrops of the adjacent Transantarctic Mountains. Microfaults in the Oligocene strata are intimately associated with injection of clastic dykes and with mineralization by diagenetic fluids. This shows that faulting was early, synchronous with dewatering and lithification of the strata, pointing to an Oligocene age. Devonian Beacon sandstone and Jurassic Ferrar Dolerite, cored at the base of the sedimentary rift fill, are extensively faulted and brecciated. We interpret this brittle deformation to most likely be associated with development of the Transantarctic Mountains Front fault zone. Two larger-scale brittle fault zones occur at ~260 and 540 metres below sea floor (mbsf) and are inferred to have normal-sense displacement of unknown magnitude. Another zone of intense shearing occurs between 790-804 mbsf, and may have resulted from either pre-lithification shear or brittle faulting at high pore pressures prior to complete lithification of the stratal sequence.

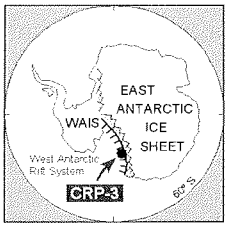

The conjugate geometry and normal-sense displacement associated with the majority of microfaults in CRP-3 core documents a vertical maximum principal stress during the Oligocene deformation. There are conjugate microfault sets with different strikes in the core, but no cross-cutting relations that establish whether the sets are coeval or formed in discrete deformation episodes. One interpretation is that development of the fault sets overlapped in time, with the orientation of the two horizontal stresses remaining approximately constant and oriented north-northeast and west-northwest, but the relative magnitudes switching with time. The strong development of the north-northeast-striking fault set indicates that the dominant maximum horizontal stress was north-northeast trending, consistent with previous interpretations invoking Cenozoic dextral transtensional shear along the Transantarctic Mountains Front boundary.

Borehole breakouts in the walls of the CRP-3 drillhole demonstrate that the present-day minimum horizontal stress direction is oriented east-northeast. The population of drilling-induced petal-centreline and core-edge fractures documented in orientated CRP-3 core yields a result ~20 degrees from this, whereas the hackle plume axes on low-angle tensile fractures in orientated core are consistent with the breakout results. The east-northeast orientation of the *in situ* minimum stress direction is perpendicular to the regional trend of the Transantarctic Mountains Front structural boundary. It is not compatible with the oblique stress orientations inferred from the natural fracture sets. One possible explanation for this is reorientation of the minimum stress direction perpendicular to the regional Transantarctic Mountains topographic gradient post-dating Oligocene tectonism.

INTRODUCTION

The Transantarctic Mountains Front is the structural boundary between the Victoria Land rift basin and the Transantarctic Mountains rift flank uplift (Barrett et al., 1995). This fundamental structural front has been modeled as a normal fault system, analogous to rift margin fault systems in the East African rift system (*e.g.*, Tessensohn and Wörner, 1991) and is inferred to have a long history of Mesozoic and Cenozoic rift-related displacements. Structural mapping along the onshore portion of the Transantarctic Mountains in southern Victoria Land has documented an array of normal faults orientated obliquely with respect to the mountain front, which have been interpreted to have accommodated transtensional motion across the rift boundary (Wilson, 1992, 1995). Based on thermochronological

*Corresponding author (wilson.43@osu.edu)

data, this oblique displacement was interpreted to occur in the Cenozoic, beginning at *c.* 55 Ma, concomitant with the principal phase of Transantarctic Mountain uplift (Fitzgerald, 1992). Because rocks exposed onshore are dominantly of Jurassic and older age, it has not been possible to obtain more firm age constraints on Transantarctic Mountains Front faulting history in southern Victoria Land. In northern Victoria Land, however, Rosetti et al. (2000) have documented faulting and McMurdo dyke emplacement of Cenozoic age in a dextral transtensional setting along the rift shoulder. Dextral transtensional deformation for the entire Ross Sea region has been interpreted by Salvini et al. (1997).

The Cape Roberts Project (CRP) drillsites are located along the offshore portion of the Transantarctic Mountains Front (Barrett et al., 1995; Fig. 1). The drillholes were sited to retrieve a section of the sedimentary strata of the Victoria Land rift basin, in order to obtain information on the history of glaciation, rifting, and mountain uplift in the region. We conducted an analysis of fractures in the core and borehole walls of the CRP drillholes to document the timing and kinematics of faulting along the Transantarctic Mountains Front, and to obtain information on the modern-day stress field along this structural boundary. Here we report on fractures logged in the CRP-3 core; borehole-wall fractures indicative of contemporary stress are described by Jarrard et al. (this volume). The types and orientations of fractures in CRP-3 core are compared with fracture sets previously documented in the CRP-2/2A cores (Wilson and Paulsen, 2000) and to Transantarctic Mountains Front fault patterns mapped in outcrop onshore (Wilson, 1995) and in offshore seismic reflection profiles (Hamilton et al., 1998, 2001).

METHODS

The CRP drilling was carried out from a floating platform of sea ice that was nearly stationary relative to the shore during the drilling period (Cape Roberts Science Team (CRST), 1998, 1999, 2000). A wireline diamond drilling system with a triple-tube coring assembly yielded *c.* 97% core recovery in CRP-3. Downhole logging with a dipmetre showed that the CRP-3 drillhole is within 1-2.5 degrees of vertical (CRST, 2000; see Jarrard et al., this volume). CRP-3 drilling recovered approximately 345 m of 61 mm diameter core (HQ) and 591 m of 45 mm diameter core (NQ). At the CRP drillsite laboratory, depths in metres below sea floor (mbsf) were assigned to the top and bottom of the core run and of each fracture. The dip and dip direction of each fracture were measured with respect to an arbitrary 'north' defined by a red line scribed the length of each core run. We systematically examined the core surface and, where open, the individual fracture surfaces to constrain fracture mode of origin. We also recorded any bedding offsets, crosscutting or abutting relations between fractures, type of fracture fill, and type and orientation of any surface fractographic features. In total, 3227 fractures of all types were logged in the *c.* 940 m of CRP-3 core.

During logging we defined intact core intervals, within which there had been no internal relative rotation of the core during drilling or coring. The boundaries of the intact core intervals were either defined by core run breaks, in cases where the top and bottom of core runs could not be fitted together, or by fractures with surfaces containing circular grooves indicating the core had spun during drilling. Approximately 55% of core runs could be fitted together, with the longest intact core intervals nearly 30 m long. After initial core processing, the core was cut in one-metre segments and a DMT CoreScan® instrument was used to scan the whole core, except where the integrity of the core did not permit handling. We were able to scan 77% of HQ and 90% of NQ whole core for CRP-3, providing an exceptional digital record of the core.

In order to orientate fractures in the core with respect to true North coordinates, the whole-core scans were digitally stitched together to reproduce the

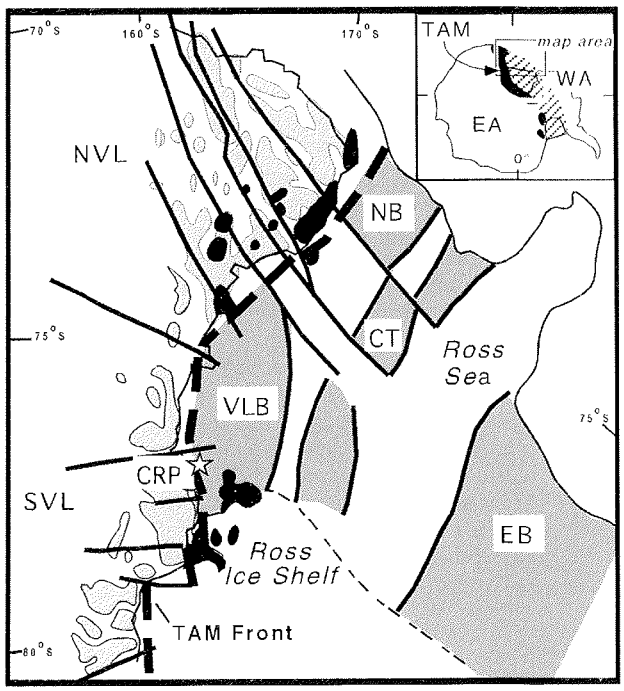

Fig. 1 - Regional setting of Cape Roberts Project (CRP) drill sites along the Transantarctic Mountains Front Zone (TAM Front), the structural boundary between the Transantarctic Mountains rift flank and the Victoria Land rift basin (VLB). SVL: Southern Victoria Land; NVL: Northern Victoria Land; NB: Northern Basin; CT: Central Trough; EB: Eastern Basin. Inset: TAM: Transantarctic Mountains; EA: East Antarctica; WA: West Antarctica. Pale grey shading denotes generalized rock outcrop in the TAM; black denotes outcrop of Cenozoic McMurdo Volcanic Group; dark grey shading denotes rift basins beneath the Ross Sea. Modified from Cooper et al., (1987), Salvini et al. (1997); Wilson (1999).

intact core intervals we had defined during core logging. The intact core intervals were reorientated to *in situ* coordinates by matching fractures, bedding, and clasts visible in the core scans with the same features in orientated borehole televiewer (BHTV) imagery of the borehole walls, using procedures presented in Jarrard et al. (this volume). The orientation of the red scribe line with respect to true North was then determined and used to correct core-based structural measurements to *in situ* coordinates. In addition, a correction had to be applied for a gradual drift in the position of the red scribe line used as 'arbitrary north' for core measurements, apparently resulting from the core scribing procedures. Orientation errors are estimated to be about $\pm 10^{\circ}$ for entire stitched core intervals and $\pm 15^{\circ}$ for individual fractures (Jarrard et al., this volume; Paulsen et al., 2000). At this time, approximately 231 m of core, or 25% of the cored interval has been reorientated; this work is still in progress. Fracture strikes discussed here refer only to those fractures that occur within orientated core.

Millan (2001) examined thin sections of 37 samples of CRP-3 core to characterize the microscopic textures of closed core fractures, including clastic dykes, veins, and microfaults. Work in progress on the microscopic textures and their relation to diagenesis holds promise in determining the relation between fracturing, fluid flux and diagenesis, and to improve our classification of natural fractures based on macroscopic logging (Millan et al., 2000).

CHARACTER AND ORIENTATION OF NATURAL FRACTURES AND FAULTS IN CRP-3 CORE

NATURAL FRACTURES

Fractures that formed by natural processes and that were retrieved in the core are referred to as 'natural' fractures. Natural fractures are distinguished from 'induced' fractures formed during drilling, coring or handling by their typical textures, similar to outcrop structures, and by distinct geometric attributes (Kulander et al., 1990). Our primary objective is to map structures formed by past and present tectonic crustal stresses, so we focussed our core logging on discrete, planar fractures that truncated any bedding or soft-sediment deformation structures visible in the core. Tectonic structures are expected along the boundary between the Transantarctic Mountain Front and the Victoria Land rift basin, where the CRP drillsites are located. However, the strata cored by CRP drilling have almost certainly been over-ridden by grounded ice multiple times, and may have been affected by rapid loading by ice-rafted debris or by downslope mass movement, so consideration of glaciotectonic and syn-depositional deformation is also important (*e.g.* Passchier, 2000; van der Meer, 2000). In this paper, we discuss natural fractures we interpret to be of tectonic origin. We note that unambiguous discrimination is not always possible, in large part because of the limitations imposed by structural mapping of a narrow, vertical drill core, which precludes application of many criteria commonly used to differentiate tectonic from glaciotectonic or other pre-lithification deformation.

BRITTLE FAULT ZONES

Several factors indicate the presence of two major brittle fault zones that likely accommodated significant offset. We refer to these fault zones as faults A and B. Both fault zones occur in Oligocene strata, fault A at *c.* 260 mbsf and fault B at *c.* 539 mbsf. At both of these depths, mainly fallback material was recovered rather than intact core. Drilling fluids were lost in large quantities, indicative of the presence of open fractures in the borehole walls. Downhole temperature logs at these depths indicate substantial fluid flow, likely reflecting fracture porosity and permeability associated with a fault zone (CRST, 2000). It is not possible to constrain displacement magnitude because no evidence of these faults is recorded at the resolution of available seismic records and because of a lack of appropriate markers in the core. Dipmeter data show that bedding dips do not change across these zones, indicating that they are nonrotational faults without detectable drag (Jarrard et al., this volume).

Fault zone A is marked by breccia recovered from 257-263 mbsf. The actual fault must lie between *c.* 260-262.5 mbsf, where the only material retrieved was brecciated and intensely veined rubble. Immediately beneath the brecciated zone, a large dolerite clast is cut by hairline calcite veins identical to those that pervade the breccia, indicating that deformation conditions were such that hard, relatively strong rock (*i.e.*, the dolerite clast) met failure conditions during faulting. This is significant because it shows that hard rock was being fractured and broken during the faulting. Instability of the borehole walls precluded logging between 256-272 mbsf, so we have no direct record of the orientation of the fault zone. However, microfault density was relatively high in the core within the 10 m intervals immediately above and below the fault zone. Microfaults in orientated core closest to the fault (~249.5-253.9 mbsf) strike north-northeast and dip steeply westward. All microfaults above and below the fault zone with definite kinematic indicators have normal-sense displacement. Most have dip-slip or steep oblique-slip lineations. One microfault has two sets of high-angle oblique-slip striae, suggesting that fault zone A accommodated multiple slip events, but no overprinting relations are preserved. In sum, fault

zone A most likely has a north-northeast, west-dipping attitude and accommodated normal displacement.

Fault zone B is marked by breccia recovered from 538-540 mbsf, a more narrow zone than fault zone A. Core was lost between 538.36-538.72 mbsf and the main fault surface must lie within this zone. A preserved part of the fault zone is characterized by sparry calcite precipitated in open voids. Here breccia fragments preserve the planar contact between sandstone and a large dolerite clast (Fig. 2), indicating that the sandstone had similar mechanical properties as the dolerite clast at the time of deformation (*i.e.*, they both deformed by brittle failure). Thus, the sandstone must have been cohesive or fully lithified by the time of deformation. A normal fault recovered from the base of the loss zone has an orientation of 065, 80 N (Fig. 2). Several normal-displacement microfaults occur within 1m beneath this fault surface and form a conjugate set, with the dominant set having an average orientation of 081, 68 N (Fig. 2). Abundant microfaults in the interval below the fault zone (540.27-562.79 mbsf) form 2 conjugate sets that strike north-northeast and west-northwest, different from the ~east-northeast strike within the fault zone. The east-northeast strike is similar to a seismically-mapped fault set across Roberts Ridge (Hamilton et al., 1998, 2001), suggesting that fault zone B may be related to that fault array.

We identified an additional zone of brecciated material, recovered only as fallback from an interval between 292.81-293.43 mbsf, which may represent a third major fault zone. However, in this case there is no increase in microfault density in the surrounding core, nor is there logging evidence of increased fracturing of the borehole walls at this depth.

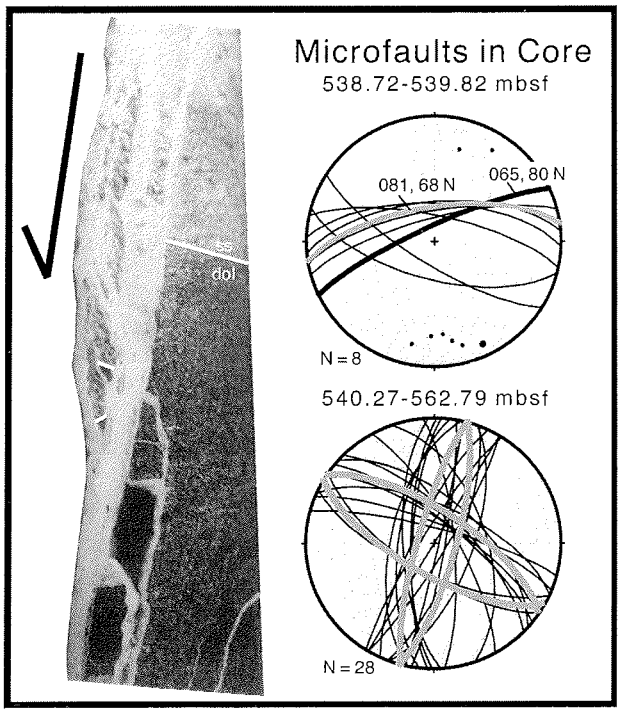

Fig. 2 - Fault with calcite veining and brecciation preserved at base of fault zone between 538-540 mbsf. Note that the sandstone (ss) / dolerite (dol) contact (white line) remains planar and undistorted in the breccia fragments, indicating faulting of fully indurated material. Core is 45 mm in diameter. Lower hemisphere, equal-area stereoplots of microfaults within 1 m below the fault zone (upper plot) and within the underlying ~20 m of core. The fault surface forming the base of the fault zone is denoted by the bold black great circle curve in the upper plot. The thick, grey great circle curves denote average orientation of fault sets.

SHEAR ZONE

A zone with evidence of significant shear occurs between ~790 and 804 mbsf. This zone has a character different than brittle fault zones and microfaults found in the rest of the core. Lithologically, this interval consists of dolerite cobbles and boulders within a matrix of sheared clay-size material. The unit has been interpreted as a conglomerate, possibly deposited in an environment like a fan-delta system in which mud accumulated intermittently (CRST, 2000). Although the evolution of this zone remains somewhat enigmatic, both macroscopic and microscopic textures indicate that the zone has undergone substantial shear and therefore marks a shear zone rather than an undisturbed *in situ* sedimentary deposit. Here we describe key structures and textures from the zone in order to place constraints on its origin and evolution.

Dolerite blocks, up to 1.92 m in vertical section, dominate the zone. Dolerite clasts cross the spectrum of size from sand to boulder (visible clasts >1m to <1mm) and of shape from rounded to sharply angular. Local 'jigsaw puzzle' fits between angular clasts indicate *in situ* brecciation of the dolerite (Fig. 3). Halos of smaller clasts envelop the cobble- to boulder-size clasts, indicating brittle fragmentation and dispersal of fragments by shear (Fig. 3). The zones of dispersed fragments grade into ultra-fine-grained material that, when broken, shows a glassy polish and ubiquitous fine slickenlines, documenting pervasive shear (Fig. 3). We interpret these fragmental zones to be breccias formed from cataclasis during shear. At least some component of the clay-sized matrix is likely to be of cataclastic origin. The presence of a pollen grain, and rare, small pebbles of mudstone and granite, indicate some of the matrix is original sediment (CRST, 2000). Clay mineralogy studies have shown that the fine matrix material is dominated by smectite, together with mixed-layer clays (Ehrmann, this volume; Setti et al., this volume). It is unclear, however, whether the clay material represents original detrital clay, if it is authigenic as seen elsewhere in the core (Wise et al., this volume), or if some of it formed during shearing and alteration of dolerite.

The breccia zones have several forms. Some have sharp, planar boundaries that are slickenside surfaces

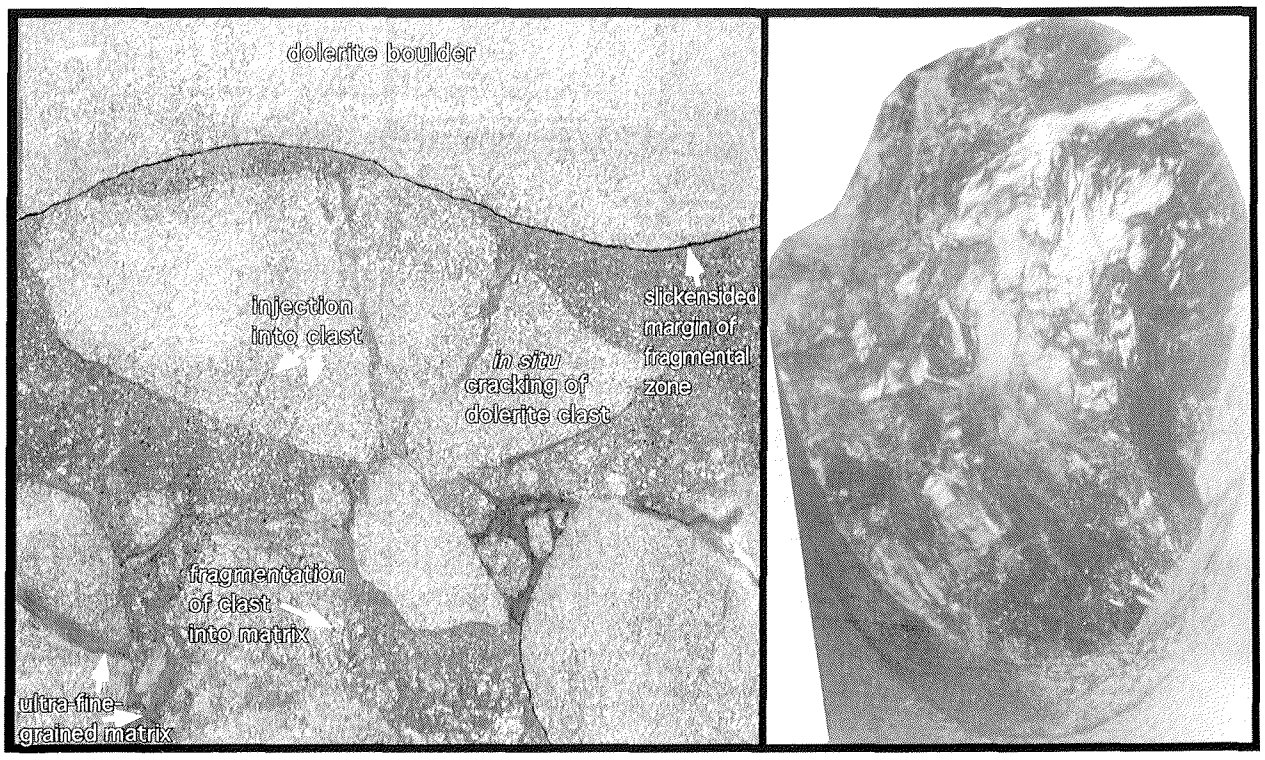

Fig. 3 - A. Brecciated zone within shear zone at 790-804 mbsf; unrolled whole-core scan is 141.4 mm across. B. Highly polished and slickenlined, black 'glassy' matrix indicating intense shear of breccia matrix. Core is 45 mm in diameter.

with low to moderate dips, whereas others are steeply dipping (Figs. 3 & 4). Irregular bodies, or zones with one planar and one irregular margin, also occur. The planar boundaries of the fragmental zones do not have any strong preferred orientation, although some are sub-parallel to the average 'bedding' plane attitude picked from BHTV and core scan analysis (Jarrard et al., this volume) (Fig. 4).

There is a variety of evidence that the brecciated material and the fine-grained matrix have flowed.

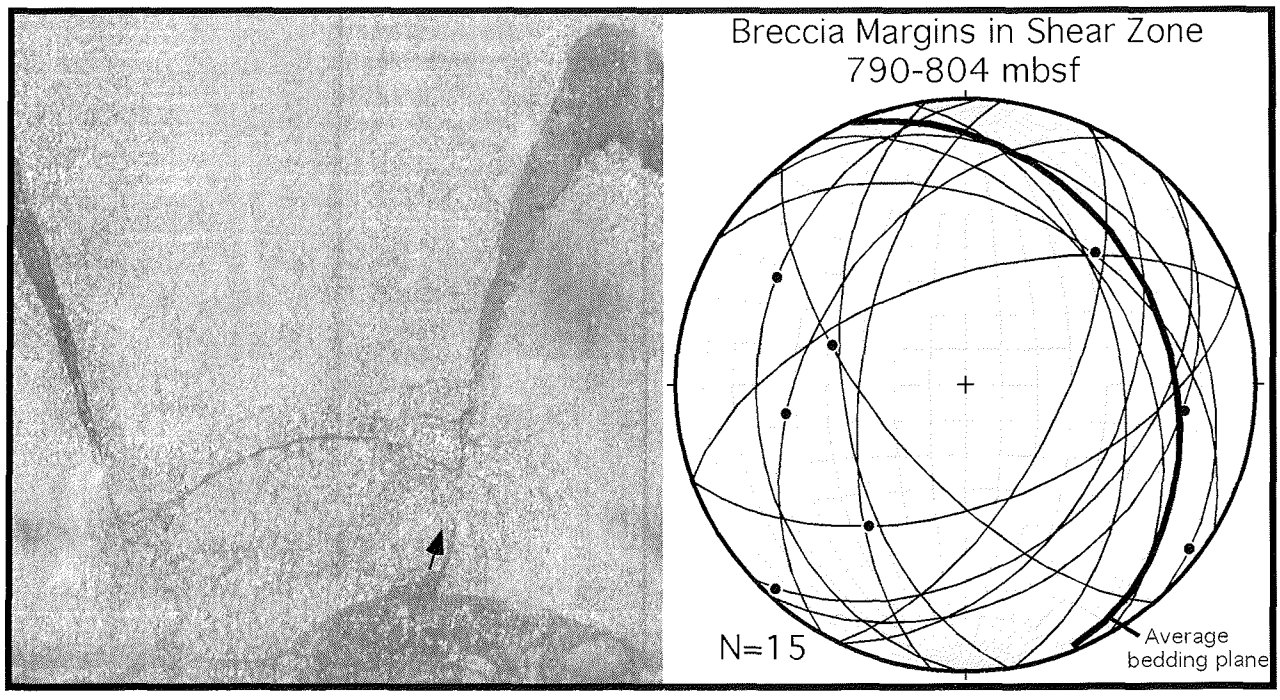

Fig. 4 - A. Steep, planar band of fine-grained breccia injected upward from moderately-dipping breccia zone; note upward injection (arrow) and thin veins of fine-grained breccia emanating from zone. Unrolled whole-core scan is 141.4 mm across. B. Lower-hemisphere, equal-area stereoplot of planar breccia margins in orientated core from the shear zone. Note parallelism of many of the margins to the 'average bedding plane' derived from analysis of BHTV and scanned core by Jarrard et al. (this volume).

Each of the geometric types of breccia is associated with 'veins' of fragmental material that branch or terminate upward or laterally, indicating injection into adjacent intact dolerite clasts (Fig. 4). The black matrix material forms wispy injections into clast interiors, partially breaking them up (Fig. 3). Ductile flow of the matrix is also indicated by microscopic flow folds in the laminated clay matrix of brecciated intervals (Millan et al., 2000).

Planar dykes of quartz sandstone cut dolerite boulders near the top of the zone and also in the less-sheared interval immediately below it (Fig. 5). The dykes have a very regular north-northwest strike and westward dip (Fig. 5). When the dikes are rotated such that average bedding is restored to horizontal, they define a sub-vertical set striking north-northwest (Fig. 5). This suggests that the dykes may be tensile fractures formed in response to east-northeast – west-southwest extension, prior to tilting of the strata.

Within the breccia zones, the fine-grained, black matrix has been intensely sheared. The matrix splits into planar-curviplanar polished and slickenlined surfaces or small, polished, phacoidal chips (Fig. 3). Microscopically, an intense preferred orientation of phyllosilicates defines a fabric parallel to these shear surfaces (Millan et al., 2000). These features strongly resemble the fabric called 'scaly foliation' formed in strongly-sheared clay-rich sediments along thrust faults in active accretionary prisms, and also found in olistostromes, melange diapirs and landslides (Moore et al., 1986). Scaly foliation has been shown to develop in unlithified mud, commonly rich in smectite, and associated with high porosity and pore pressure (Moore et al., 1986). Unlike the present case, however, only minimal cataclasis and no injection features have been described from zones with scaly foliation.

Discrete faults with black, highly polished and slickenlined surfaces, similar to the shear surfaces in the breccia matrix, cut the large dolerite blocks within the zone. These discrete faults and the planar, slickenlined surfaces within the breccia matrix vary from steep to low-angle dips, with slickenline orientations indicating oblique shear (Fig. 6). Many of these shear surfaces are parallel to the average 'bedding' plane determined from dipmeter, BHTV and core-scan analysis by Jarrard et al. (this volume) (Fig. 6). When the shear surfaces are rotated such that average bedding is restored to horizontal, the low-angle subset becomes subhorizontal, consistent with bedding-parallel shear. The high-angle shear surfaces either strike NNW or NE (Fig. 6), similar to the typical orientations of microfaults in Oligocene strata, described below. Slip on the shear surfaces is oblique, rather than dip-slip, however. There has also been shear along the margins of some of the clastic dykes within the zone, indicated by slickenlines or fibers, and both the dyke margins and their slip directions are similar to the NNW shear surfaces (Fig. 6). For *c.* 20 m below the main shear zone, dolerite clasts are cut by faults with black, polished surfaces and slickenfibres and by clastic dykes with similar orientations and kinematics as in the 'shear zone'.

In sum, some deformation features within the shear zone show evidence for pre-lithification deformation, whereas others show evidence for brittle failure of hard rock. We consider here two possible models that may account for this apparent dichotomy

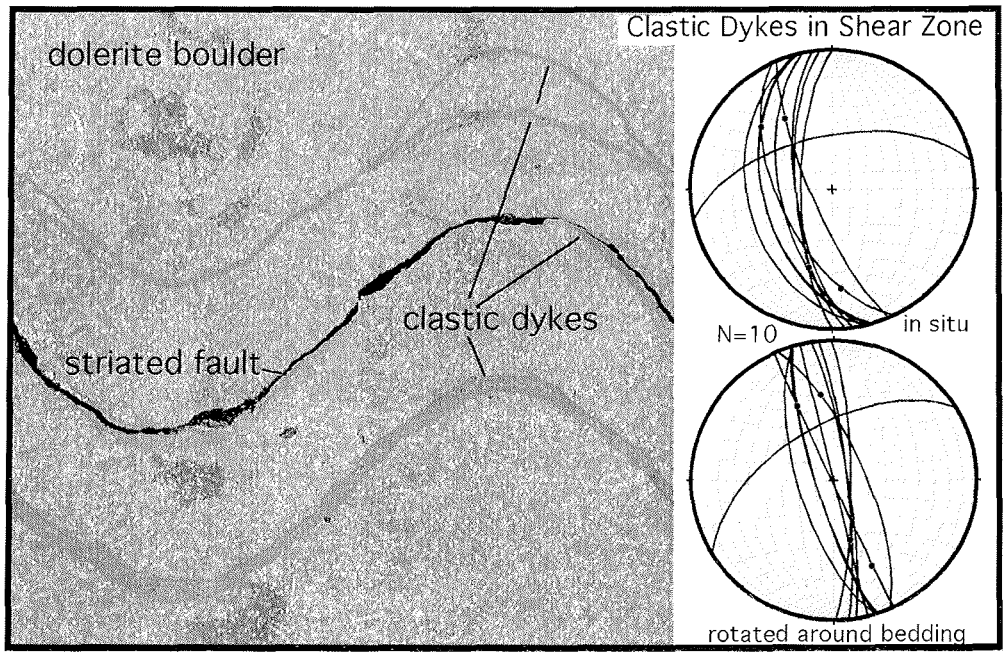

Fig. 5 - A. Parallel set of clastic dykes and a slickensided microfault cutting a dolerite boulder within the shear zone at 790 mbsf. Unrolled whole-core scan is 141.4 mm across. B. Stereoplots of clastic dyke attitudes before (upper) and after (lower) rotation to restore 'average bedding' to horizontal. Equal-area, lower-hemisphere plots.

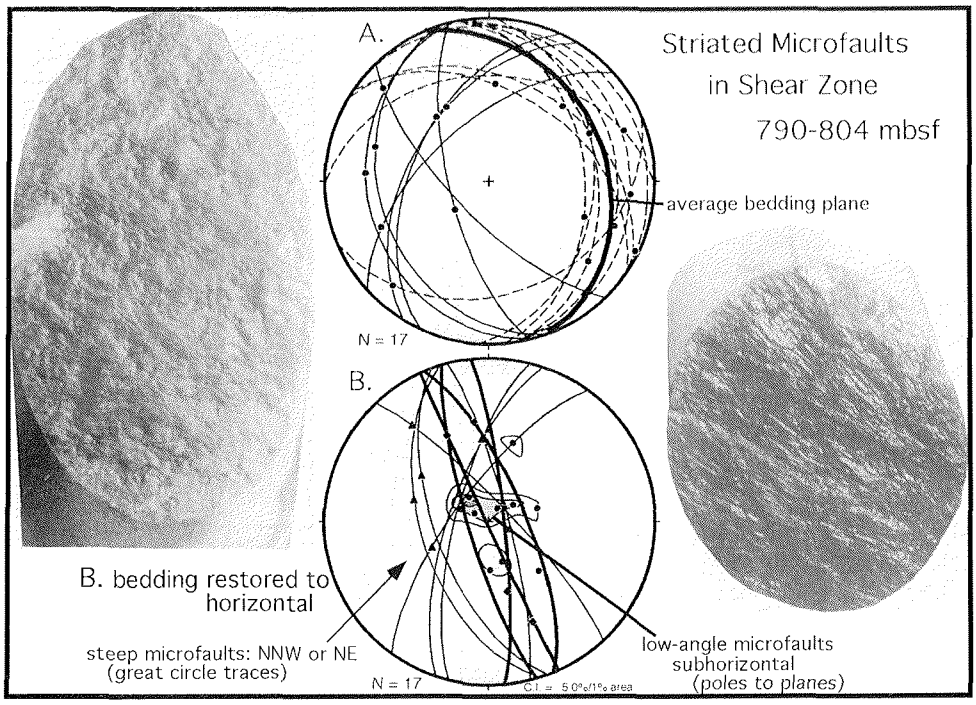

Fig. 6 - Photographs and stereoplots showing both steep and shallow microfaults with oblique shear within the 790-804 mbsf 'shear zone'. Stereoplot A. shows microfault planes (great circle curves) and striae (black dots) in *in situ* coordinates; the bold great circle is 'average bedding plane' based on Jarrard et al. (this volume). The dashed great circles are microfaults subparallel to the average bedding plane. Stereoplot B. shows the same faults and striae (triangles) after rotation to restore bedding to horizontal. In B, low-angle microfaults are plotted as contoured poles (corresponding to planes shown as dashed great circles in Stereoplot A), showing subhorizontal attitude after rotation. Steep microfaults and clastic dykes (bold great circle curves) with slip lineations (triangles) form a dominant northwest-striking conjugate set, with some northeast-striking planes, similar to fault patterns in overlying Oligocene strata. Equal-area, lower-hemisphere plots. Core in photos is 45 mm in diameter.

of results. In the first model, the main shearing occurred before the strata were lithified. The presence of clastic dykes clearly shows that sediments proximal to the zone were unlithified and under substantial pore fluid pressures. The resemblance of the breccia-matrix fabric to scaly foliation suggests it could have formed in unlithified mud. Together the presence of sedimentary dykes and possible 'scaly foliation' can be interpreted to reflect shearing prior to lithification of the sequence. The parallelism of some of the shear surfaces and 'bedding' in the zone could be consistent with shearing during down-slope mass motion, or shear may have occurred along a low-angle fault zone and the inferred 'bedding planes' may in fact all be shear surfaces. A later event would then have reactivated pre-existing fractures by oblique shear and produced the high-angle faults in the zone.

In the second model, brittle shear of lithified material was dominant. High pore-fluid pressures were locally preserved in high-porosity sands, while the rest of the sequence was dewatered and mostly or completely lithified. The clast-supported dolerite blocks broke at their contacts and continued to crush and fragment as they interacted during shear. High pressures in the fine-grained matrix, both original mud and cataclastic debris, mobilized the breccias to form injections and facilitated brittle cracking of the dolerite. The evidence for *in situ* brecciation and development of at least some of the fine-grained matrix by cataclasis is consistent with this model. Because breccias were injected in dyke-like and irregular forms, there must have been substantial internal pressure during the shear deformation. Injection of fine, cataclastic material is known from faults where high-slip-rate events are associated with transient high pressures. A single brittle shear event would require oblique shear kinematics to form the diverse slip lineations observed.

Unfortunately, there are no cross-cutting relations between shear surfaces and clastic dykes, between shear surfaces with steep and low-angle dips, or between breccia zone margins and shear surfaces, to establish relative timing and constrain these alternative models. We note that one interpretation of seismic reflection profiles suggests that CRP-3 may have cored a steeply-dipping fault at approximately this level (Hamilton et al., 2001), although an alternative interpretation is that no faults are resolved by the seismic profiles (CRST, 2000; Henrys et al., this volume).

NATURAL FRACTURES IN LOWER OLIGOCENE STRATA

Fracture Types

Planar fractures that transect the entire core and form zones of mm-cm breadth are very abundant throughout the Oligocene section of the CRP-3 core.

Here we discuss those that we could classify as natural fractures based on textures, fill material, or association with definite natural fractures. We exclude a population of planar fractures of 'indeterminate' origin that could either be natural or induced in origin. During core logging, the natural fractures were categorized as microfaults, veins, or clastic dykes. It is important to note, however, that these categories overlap for two reasons. First, the great majority of demonstrable faults are also mineralized, dominantly by calcite. Second, textures visible on the whole-core surface were commonly insufficient to unambiguously distinguish carbonate-cemented faults from fine-grained clastic dykes in cases where bedding was not present to identify offset (Millan et al., 2000; Millan, 2001).

Microfaults include planar fractures with truncation and offset of bedding of a few cm or less, and open, polished and grooved slickenside planes (Figs. 7a & 7d). Fractures were classified as 'probable' faults where they occur parallel to, and within a few cm of, definite fault surfaces. Planar fractures with dips in the 55-80 degree range, where no bedding or nearby faults were present, were classified as 'possible' faults. Typically the microfaults were also filled by calcite or had surrounding 'halos' of carbonate 'cement' (Fig. 7b). All microfaults, with and without vein material, were grouped for orientation analysis; only the definite and 'probable' faults are considered.

Veins are defined here as planar fractures sealed by precipitated fill or cement, with no visible offset of bedding planes. In the Oligocene strata there are two main types. Discrete veins, from <1 to 10 mm thick, composed of calcite and, less commonly, pyrite, are common. Also common are diffuse grey bands of carbonate cement along planar fractures. Both of these vein types typically dip at moderate angles, and commonly form conjugate sets (Fig. 8a). This geometric relationship, together with the ubiquitous spatial association of veins and microfaults, indicates that most formed by precipitation of vein material during faulting or along pre-existing fault planes. Sparry calcite occurs in open void space along some fault planes, indicating calcite precipitated in tensile openings formed during fault displacement (Fig. 7c). More rarely, calcite veins are compound with multiple, thin strands, or have en echelon geometry, indicating they filled tensile cracks. In some of these veins, precipitation during tensile opening is documented by calcite fibres orientated perpendicular to vein walls (Millan, 2001).

Clastic intrusions (dykes) occur in the Oligocene section of the core, filling fractures with dips between 40 and 75°. The clastic dykes range from 3 to 10 mm thick and typically have sharp and planar boundaries, although some have irregular shapes. Dykes are commonly cemented with calcite and/or pyrite. Our initial core logging underestimated the abundance of clastic dykes, because this carbonate cementation gives rise to the appearance of the dykes as 'grey carbonate cement bands' on the whole-core surface. Millan (2001) has shown that many of these bands are fine-grained clastic dykes, with a matrix of calcite and pyrite. There is clear evidence that some clastic dykes were injected along fault planes (Millan et al., 2000).

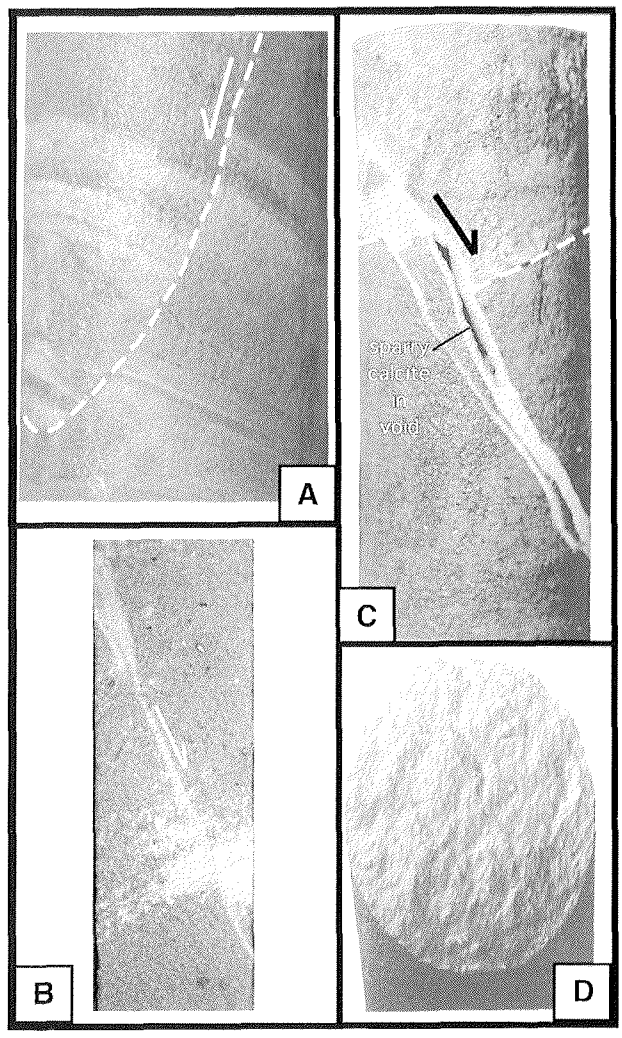

Fig. 7 - Typical microfault and calcite vein types in CRP-3 core. A: Closed microfault offsetting bedding, 61 mm diameter core; B: Photo of slabbed core showing 'carbonate cement band' along fault plane; core 45 mm diameter; C: Normal fault with sparry calcite in open, dilational void along fault plane; core 61 mm in diameter; D: Polished and lineated slickensided normal fault; core 45 mm in diameter.

Orientation

Microfaults, veins, and clastic dykes in orientated intervals of CRP-3 core define at least two, and probably three, sets with north-northeast, northwest, and approximately east-west strikes. To identify any pattern of vertical spatial distribution of the sets, fractures have been plotted for each orientated intact interval and also in sections up to ~50 m long, consisting of independently orientated intact intervals

that form nearly complete composite sections. In many intervals, two or three different conjugate sets striking NNE, NW, or WNW to ENE are present. In other intervals, one of the sets is well developed, with only rare members of the other sets. Based on available data, it does not appear that any set is spatially restricted to discrete intervals of Oligocene strata. Representative populations from selected orientated intervals are described here.

In the interval from 404-413 mbsf, microfaults form a well-defined NNE-striking conjugate set, with dip-slip or high-angle oblique-slip motion indicated by striae orientations (Fig. 8). Calcite veins also form a NNE-striking conjugate set, with a few scattered in WNW or ENE strikes. The association of thin calcite veins with normal faults, their conjugate geometry and local cross-cutting relations (Fig. 8) indicate that the veins formed along normal fault planes.

The interval from 610-666 mbsf has mainly NW-striking microfaults (Fig. 9). The majority of these faults have approximately dip-slip striae and all have calcite mineralization. Conjugate geometry and mutual offsets are present. The microfaults occur in closely-spaced groups of 3-6 within zones from 10 to 150 cm in extent, separated by sections up to 8 m in length with few or no microfaults. One sub-interval *c.* 1.5 m long has four closely-spaced microfaults that define a set with a west-northwest strike and southwest dip. A few microfaults with NE strikes are scattered through this interval.

Microfaults in the interval between 204-254 mbsf are orientated in sets with NW, NE, and E-W strikes, with those with NW strike and northeasterly dip most common (Fig. 10). Fractures logged as calcite veins, grey 'cement bands' or clastic dykes also define 3 sets with similar orientations, with NNE-striking and southeasterly dipping planes most abundant (Fig. 10). These two categories clearly overlap in both morphology and geometry. In some cases, calcite veins and clastic dykes have well-developed conjugate geometry, typical of normal faults. Many of the faults with striae or bedding offset were also mineralized by calcite. This indicates that the calcite mineralization and the clastic intrusions were localized along normal

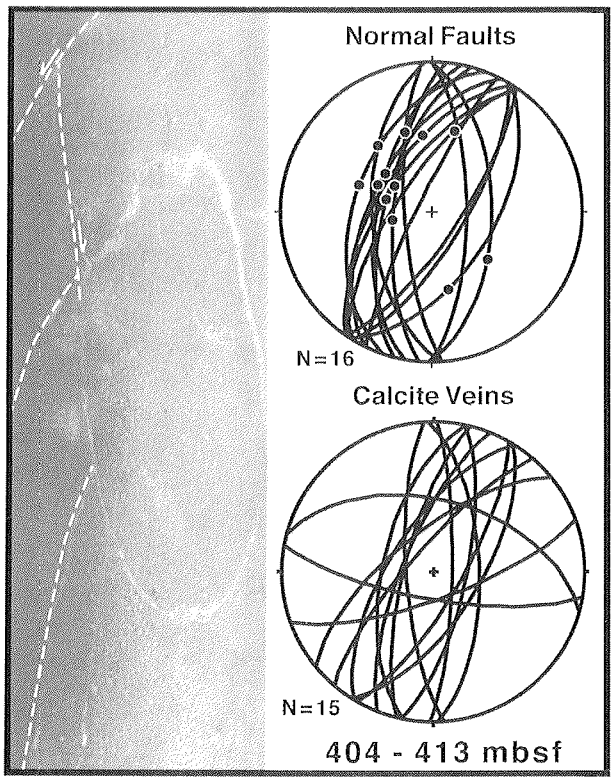

Fig. 8 - Microfaults and veins in orientated core interval between 404-413 mbsf. Photograph of 'hairline' calcite veins forming a conjugate array with mutual offset relations, documenting mineralization along faults. Upper stereoplot shows well-defined north-northeast striking set of conjugate normal faults with steep slip lineations (dots on great circle traces); lower stereoplot shows similar pattern of calcite veins. Equal-area, lower-hemisphere plots. Core is 45 mm in diameter.

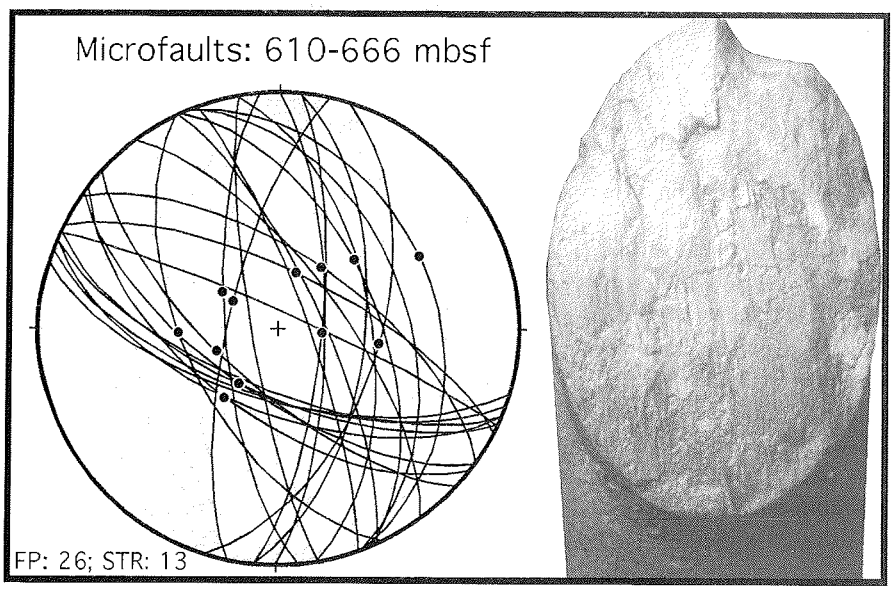

Fig. 9 - Microfaults in orientated core interval between 610-666 mbsf. Photograph shows polished surface with calcite slickenfibres documenting normal-sense, dip-slip displacement. Stereoplot shows dominant northwest orientation and conjugate geometry of faults in this zone. Equal-area, lower-hemisphere plots. Data numbers given as FP=fault planes and STR=striae. Core is 45 mm in diameter.

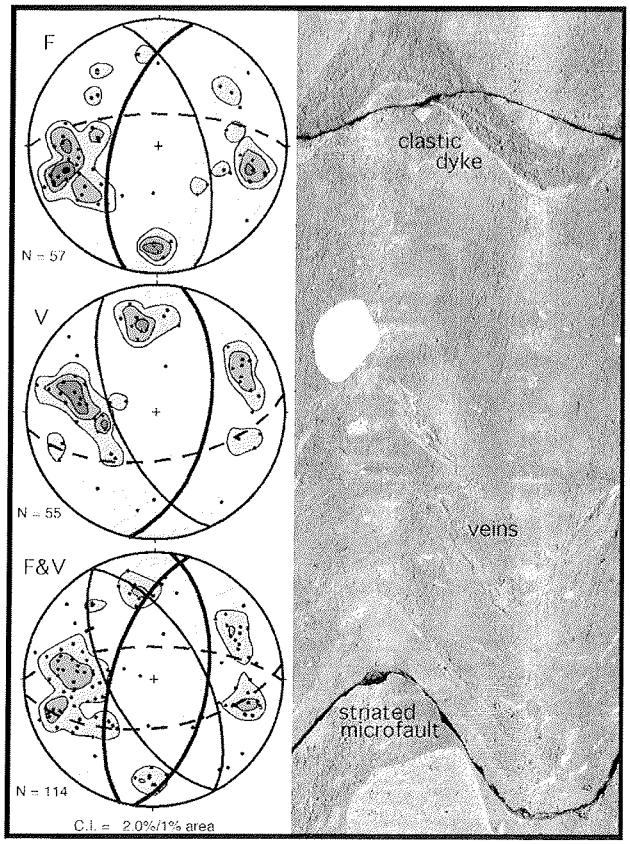

Fig. 10 - Parallel microfaults, calcite veins and clastic dykes in orientated core interval between 204-254 mbsf. Upper stereoplot (F) shows normal-displacement microfaults; center stereoplot (V) shows veins and clastic dykes; lower stereoplot (F&V) combines these fracture types. Note that north-northeast, northwest, and ~east-west conjugate fracture sets are all present in this interval. Equal-area, lower-hemisphere plots; bold great circles are average fracture planes selected from contour maxima. Unrolled whole-core scan is 191.6 mm across.

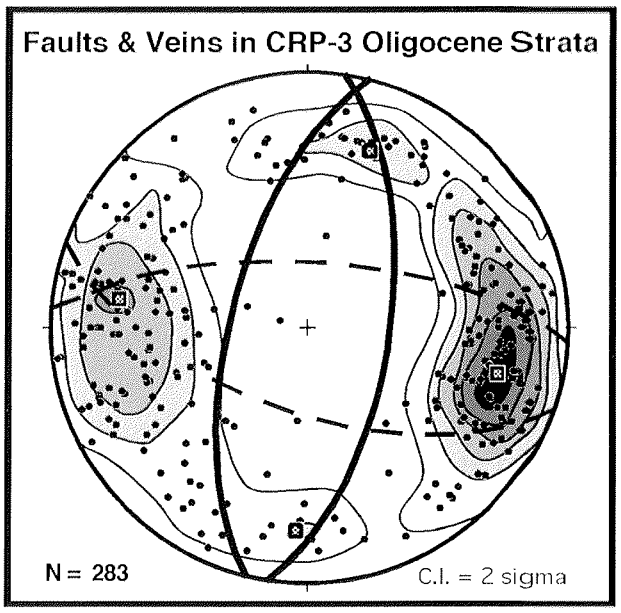

Fig. 11 - Summary stereoplot showing the attitudes of faults and veins in orientated core from CRP-3 above the 'shear zone' at 790 mbsf. Dominant sets are north-northeast and close to east-west; note northwest-striking faults are present but more scattered in orientation. Equal-area, lower-hemisphere plots; great circles denote average orientation of fracture planes in core, grey squares denote corresponding average poles.

fault planes. When all the natural fractures in this interval are plotted together, the NW, NNE, and E-W sets are clearly delineated, each defined by a conjugate fracture array (Fig. 10).

In each of these examples, the microfaults, calcite veins and clastic dykes are not uniquely associated with a single preferred orientation but, instead, each forms a component of the NW, NNE and ~E-W sets. It is probable that the injections and mineralization were either synchronous with faulting or followed pre-existing fault planes. We therefore combine all these natural fracture types to look at the overall orientation of faults in the Oligocene strata at the Cape Roberts drillsite. A plot of all the natural fractures in orientated intervals of CRP-3 Oligocene core above the inferred shear zone at 790-804 mbsf is presented in figure 11. The dominant fault orientation is north-northeast-striking with westerly dip. A less-well-developed, easterly-dipping conjugate fault set is present. There are abundant faults with northwest strikes, but these structures are less strongly orientated. The contour plot shows concentrations defining a conjugate array of west-northwest striking faults.

NATURAL FRACTURES IN DEVONIAN BEACON SUPERGROUP STRATA

Fracture Types

Microfaults are abundant throughout the cored interval of quartz sandstone between 823 mbsf and the base of the core, which, based on lithological characteristics, is interpreted to be Devonian Beacon Supergroup strata (CRST, 2000). Unlike microfaults in Oligocene strata, those cutting Beacon sandstone show both normal- and reverse-sense displacement of bedding planes (Fig. 12). Just over two thirds (68%) of the microfaults with bedding offset have normal-sense displacement. Most commonly the microfaults are closed, so few striae are exposed. The observed striae have high- to low-angle oblique rakes on the fault surfaces. The oblique-slip lineations, the general parallelism of reverse and normal microfaults (Fig. 12), and the small-magnitude offsets, together are most consistent with both the reverse- and normal-sense displacements being the result of oblique shear. The dominant displacement sense was normal-oblique shear.

The largest population of natural fractures cutting the Beacon sandstone consist of fractures either filled with fine-grained clay material, or filled with coarse-grained material of clastic appearance with a high content of clay matrix (Fig. 13). The same types of fill occur along definite microfaults with bedding offset and along fractures that truncate bedding but show no discernible displacement. This apparent lack

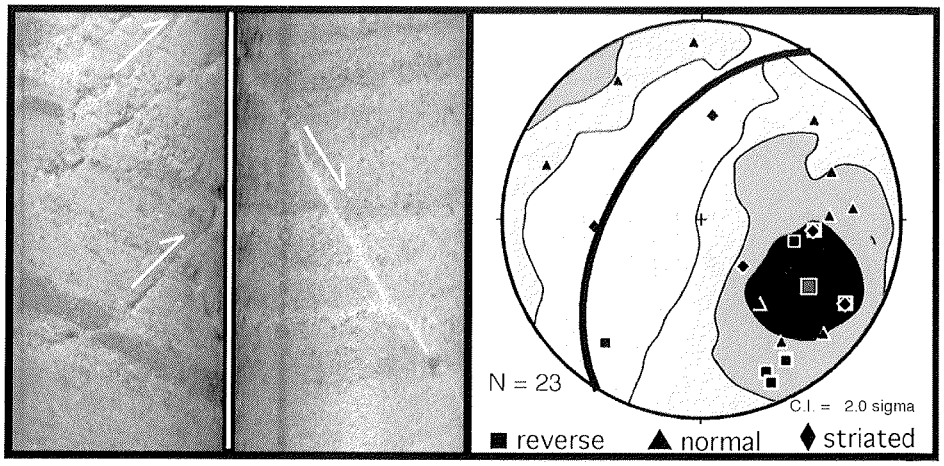

Fig. 12 - Reverse- and normal-displacement microfaults in Devonian Beacon sandstone. Stereoplot shows that reverse, normal and slickensided faults have sub-parallel, northeast-striking and northwest-dipping orientations. Equal-area, lower-hemisphere plot. Great circle trace is average fault plane orientation. Core is 45 mm in diameter.

of displacement is due to the lack of visible bedding marker planes, or may be ascribed to the large width of the fill relative to the typically small offset magnitudes. During initial core logging we considered that the fracture fill could be of either cataclastic or clastic (*i.e.* sedimentary injection) origin. However, our preliminary microstructural analysis shows that these zones are characterized by finer grain size, greater range of grain size, and more angular grains than the adjacent host rock, which we interpret as indicating cataclastic grain-size reduction (Millan et al., 2000). The abundant clay matrix within them may be partly cataclastic in origin, but most likely a significant proportion is derived from alteration of the detrital feldspar component in the sandstone by hydrothermal activity that affected this part of the core (CRST, 2000). Clasts in the fracture fill are clearly derived from the host quartz arenites. Given the Devonian age of the strata, they must have been fully lithified when these fractures formed and, therefore, sedimentary injections are unlikely. The fact that the majority of the filled fractures have a strong preferred orientation parallel to the definite microfaults with bedding offset is consistent with their formation as faults (Fig. 13).

Brecciation has affected approximately 36% of the Beacon strata in the core (CRST, 2000). Beacon fragments with angular to subrounded shapes float in a matrix of coarse sand-sized material derived from the host rock (Fig. 14). Rotation of planar bedding between clasts within the breccia documents post-lithification fragmentation. Rotation of bedding on a larger scale within the Beacon is present and is appears to be associated with this brecciation (Jarrard et al., this volume). Whole-core observations indicate that most of the breccias are planar bodies with sharp margins and steep dips that truncate bedding (Fig. 14). This suggests the breccias may mark fault zones. In addition, however, the breccias locally branch into steep dyke-like bodies crossing bedding (Fig. 14) or sill-like bodies parallel to bedding, suggesting that some of the breccias were injected.

The breccias in the Beacon strata may have formed by faulting. Where Devonian Beacon rocks crop out in the Transantarctic Mountains, however, discrete faults are present but are not associated with extensive brecciation (Korsch, 1984; Pyne, 1984; Morrison, 1989; Wilson, 1993). Therefore, if the breccias in the core are fault-related, their extensive development is most likely due to the structural position of the cored Beacon strata along the Transantarctic Mountains Front. Alternatively, the breccias could have formed under high fluid pressure conditions at the time of intrusion of the inferred Jurassic Ferrar Dolerite body. Ferrar Dolerite intrudes the Devonian Beacon strata extensively in the Transantarctic Mountains. Hydrothermal alteration associated with the dolerite emplacement is well documented there (Craw and Findley, 1984), but development of breccias in mountain outcrops has only been observed where the Jurassic dolerite intrudes the uppermost, Permo-Triassic portion of the Beacon Supergroup (Grapes et al., 1974; Korsch, 1984; Elliot, 1998), not in Devonian Beacon strata. Based on the steep, planar form of the breccia bodies, their occurrence in strata that are cut by abundant fractures and faults, and the absence of intrusion-related breccias in Devonian Beacon strata in the Transantarctic Mountains, we tentatively favor the interpretation that the breccias in the core are fault-related.

Orientation

The microfaults and filled fractures interpreted as cataclastic faults have a strong preferred orientation, with a northeast strike and a moderate dip to the northwest (Figs. 12 & 13). Compared to the faults and fractures cutting Oligocene strata, this orientation is similar, but the strike is more easterly and the dip angle is shallower. Unlike the natural fractures in the Oligocene strata, conjugate geometry is nearly absent in the fractures cutting the Beacon strata. In addition to the prominent northeast fault set, there are weak concentrations of northwest-striking fractures

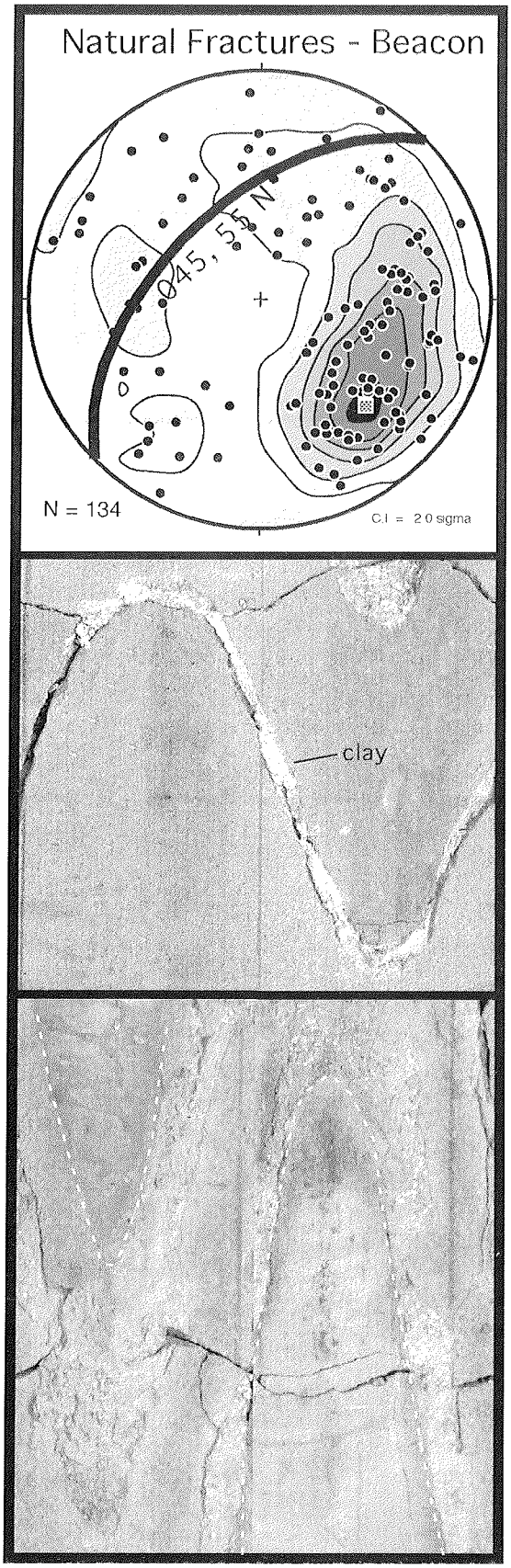

Fig. 13 - The most common natural fractures in Devonian Beacon sandstone are filled by clay (middle) or coarse-grained clastic material with clay matrix (lower); unrolled whole-core scans are 141.4 mm across. Note that the dominant orientation of these fractures is northeast, with northwest dip, parallel to the microfaults in the Beacon shown in Figure 12. Equal-area, lower-hemisphere plot.

(Fig. 13), similar to the fracture pattern in the Oligocene section higher in the core (Fig. 11). Though we have few orientated data from the breccia margins, they appear to be broadly parallel to the other natural fracture planes cutting the Beacon strata (Fig. 14).

FAULTING OF JURASSIC? PORPHYRY INTRUSION

A very strongly altered igneous body is present between 901 and 920 mbsf. The porphyry body is subparallel to bedding and is interpreted to intrude the Beacon strata (CRST, 2000). The intrusion is bounded by *in situ* volcanic breccias that parallel the contact. Though the heavily altered igneous material could not be directly dated, Cretaceous apatite fission-track ages were obtained from adjacent Beacon strata, suggesting that the intrusive body is most likely Jurassic Ferrar Dolerite (Fitzgerald, this volume), which forms voluminous intrusions within Beacon Supergroup strata in the Transantarctic Mountains. The porphyry intrusion is cut by a large population of slickensided microfaults. The microfault surfaces are associated with strong red and green coloration due to the heavy alteration of the porphyry. The faults all show low-angle oblique to strike-parallel slip lineations (Fig. 15). Because the breccias bounding the top of the intrusion caused major instability of the borehole walls, no BHTV imagery was obtained from the porphyry or underlying Beacon strata. However, the uppermost 3 m of the porphyry occur in an orientated intact interval. The 6 faults within this zone define a subparallel group with east-northeast strike and northward dip (Fig. 15).

TIMING OF NATURAL FRACTURE DEVELOPMENT

Textures, Microstructures and Diagenetic History

Where microfaults and veins cross contacts between dolerite clasts and sedimentary host without changing trend or texture, then these fractures can be interpreted as developing in either dewatered sediment with high cohesion or in fully lithified sedimentary rock. We have shown that the larger-scale fault zones and associated microfaults and veins that cut the Oligocene strata fall into this category. In addition, the microfaults characterized by calcite precipitated in open void space along the fault planes represent the same lithified mechanical state. The abundant syntectonic calcite vein material precipitated along the faults also indicates that high pore-fluid pressures had a significant role in brittle deformation. The brecciation and fault-related cataclasis of the Devonian Beacon sandstones, and the faulting of the Jurassic(?) igneous porphyry that intrudes it, are clearly hard-rock phenomena.

As previously noted, clastic dykes and calcite

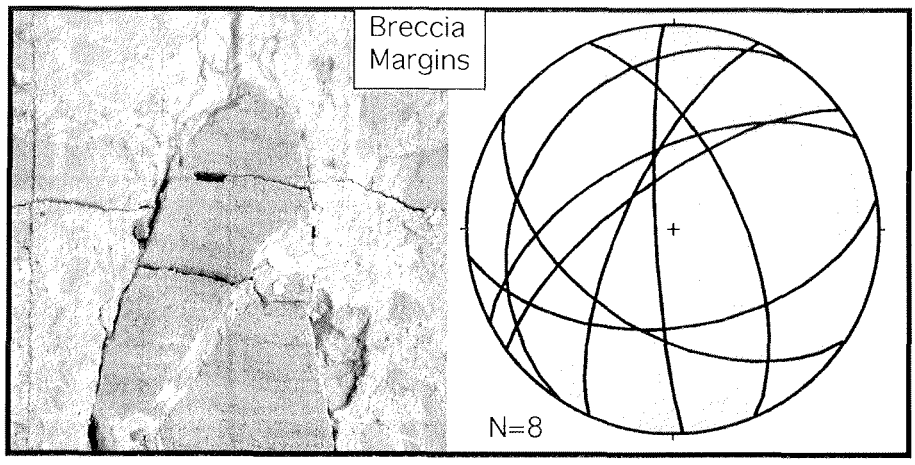

Fig. 14 - Planar breccia zone in Beacon sandstone. Note sharp, planar margin truncates bedding in sandstone and that a steep 'dyke' of breccia emanates from the margin; unrolled whole-core scan is 141.4 *mm across. Stereoplot* shows that the majority of planar breccia margins have attitudes similar to other natural fractures in the Beacon (*cf.* Fig. 13). Equal-area, lower-hemisphere plot.

mineralization occupy microfault planes throughout the Oligocene interval of the core. In general, the textural relations point to either coeval faulting and dyke injection or vein precipitation, or to injection or replacement along pre-existing microfault planes. Where clastic dykes follow microfaults, the sedimentary sequence must have been sufficiently cohesive to fracture, but some intervals remained unlithified and retained sufficient internal pore-fluid pressure to be mobilized. Initial microstructural observations show that clastic dykes are significantly more abundant than macroscopic logging had implied (Millan et al., 2000; Millan, 2001). Therefore we infer that a substantial population of the microfaults likely formed in the Early Oligocene, shortly post-dating sedimentation and coeval with dewatering and diagenesis of the sedimentary sequence. The abundance of carbonate 'cement' and vein material along the microfault planes clearly shows that the microfaults were present during diagenesis. F. Aghib (personal communication) has established that 'early' diagenetic minerals include low-Mg calcite, authigenic siderite and authigenic zeolites, whereas 'late' minerals are smectites and sparry, low- or no-Mg calcite. More detailed textural and isotopic work is needed to determine if it is possible to associate a particular type or orientation of microfault with any discrete diagenetic stage.

The interval between 204-254 mbsf was examined in detail to determine if clastic dykes, veins or microfaults of different types had any preferred orientations. Structures logged as 'clastic dykes' lie within the E-W set. Planar fractures mineralized by carbonate cement most commonly belong to the E-W and NE sets, but a few also trend NW. Striated faults most commonly strike NW and NE, with only one within the E-W set. Faults that are associated with brecciation and calcite growth in open void space and, hence, clearly formed in lithified material, are found in both the NE and E-W sets. In sum, in this interval there is no consistent association of fracture type with a single geometric set. Clastic dykes and pre-lithification faults are most common in the east-west or northeast sets, but brittle, post-lithification faults also have this orientation.

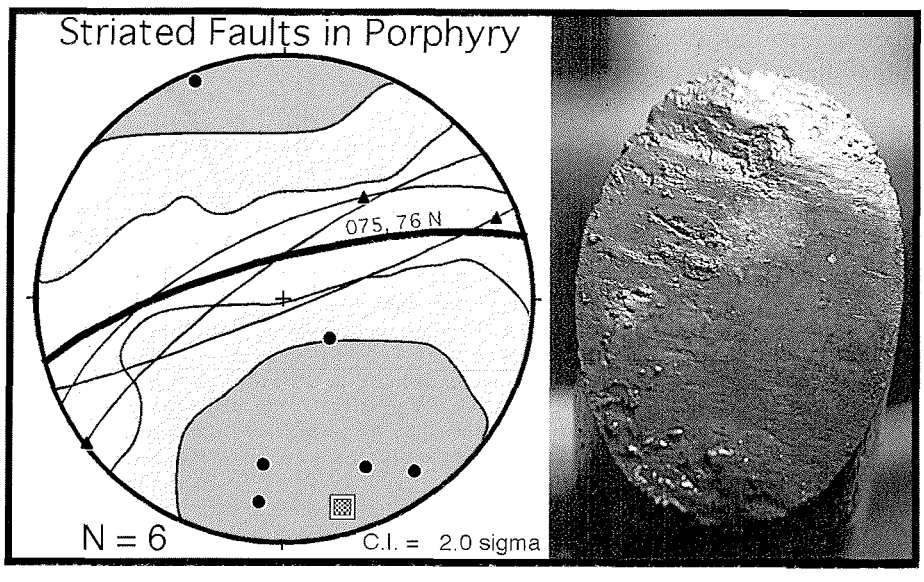

Fig. 15 - Polished and lineated microfaults are pervasive in the intrusive porphyry body, inferred to be Jurassic Ferrar Dolerite. The 6 microfaults in orientated core (black dots are poles to planes) define a subparallel group striking east-northeast; bold great circle denotes average microfault, square is corresponding average pole. The low-angle slip lineations (triangles on great circles) are typical of microfaults in the porphyry. Core in photo is 45 mm in diameter.

Relation to Hydrothermal Activity

Microfaults, fracture-fill material, and breccias in the Devonian Beacon strata have undergone extensive hydrothermal alteration. The ubiquitous microfaults within the porphyry intrusion have also been pervasively altered. An obvious candidate to drive the hydrothermal activity is the igneous intrusion itself. Because the intrusion is interpreted to be Ferrar Dolerite of Jurassic age (Fitzgerald, this volume; Pompelio et al., this volume), this would require that the hydrothermal activity occurred in the Jurassic at the time of intrusion. This would imply that the microfaults cutting both the intrusion and the Beacon strata must be Jurassic, or possibly older in the case of the Beacon structures. The fact that most of the known and inferred microfaults in the Beacon strata are approximately parallel to the dominant microfaults set in the overlying Oligocene strata, would appear to contradict this interpretation, because it seems unlikely that a Jurassic fault set and an Oligocene fault set would be so well aligned. It seems more likely that all the northeast faults would have formed in the same overall rifting event, in Oligocene or younger times. If this is the case, then young hydrothermal activity must have occurred. At this point it is not clear how hydrothermal activity associated with brecciation and faulting of the Devonian and Jurassic 'basement' of the basin fill might be linked with the mineralization above in the Oligocene section. Future isotopic work on vein material may shed light on this important issue.

Cross-cutting Relations

Microfaults, and veins interpreted as mineralized microfaults, commonly show conjugate geometry and mutual cross-cutting relations, indicating synchronous development. Conjugate relations were not uniquely associated with any one of the fracture sets defined based on orientation in the Oligocene strata. Fractures in the Beacon strata do not show conjugate geometry or cross-cutting relations.

Due to the sampling bias imposed by the vertical core, few cross-cutting relations between the fractures were observed. For example, in the interval between 204-254 mbsf, only four cross-cutting relationships were observed. In three of four, NW-striking faults cut and displaced either NE or E-W structures. In the other case, a NE fault cut and displaced an array of E-W striking bands that are probably clastic dykes. If representative, these relations suggest the E-W fractures are the oldest and the NW faults are the youngest of the three geometric sets. However, a simple age sequence such as this is not supported by the textural evidence discussed above.

Fault Attitude *vs.* Bedding Dip: Tilt Test

Jarrard et al. (this volume) have shown that the main episode of east-northeast stratal tilting began in the late Early Oligocene and ended by the Early Miocene, based on the observation that bedding dips define a fanning array from uppermost CRP-3 core through upper CRP-2A core. We can use this as a reference frame for evaluating the relative timing of faulting and stratal tilting. We have used the average orientation of bedding from Jarrard et al. (this volume) to apply a rotation to restore average bedding to horizontal, revolving bedding and fractures around the average line of bedding strike. Figure 16 shows the results for all orientated natural fractures in Oligocene strata from CRP3 core above the 'shear zone' at 790-804 mbsf and in Devonian Beacon strata between 823-901 mbsf.

The faults and fractures in Oligocene strata form well-defined conjugate sets with 60-70 degree dips in their *in situ* unrotated orientations. The clear conjugate geometry of the dominant NNE-striking fault set is distorted upon rotation to restore bedding to horizontal, suggesting that these faults formed after tilting of the strata (Fig. 16). This would imply a Late Oligocene or younger age for the microfaults.

Northeast-striking, northwest-dipping microfaults and fractures are predominant in Beacon strata. This fault set has an average attitude of 046, 55N before rotation, and is restored to an attitude of 031, 68W when bedding is rotated to horizontal (Fig. 16). The restored attitude is more typical of normal fault dips, consistent with the displacement sense on the majority of the microfaults. This suggests that the dominant

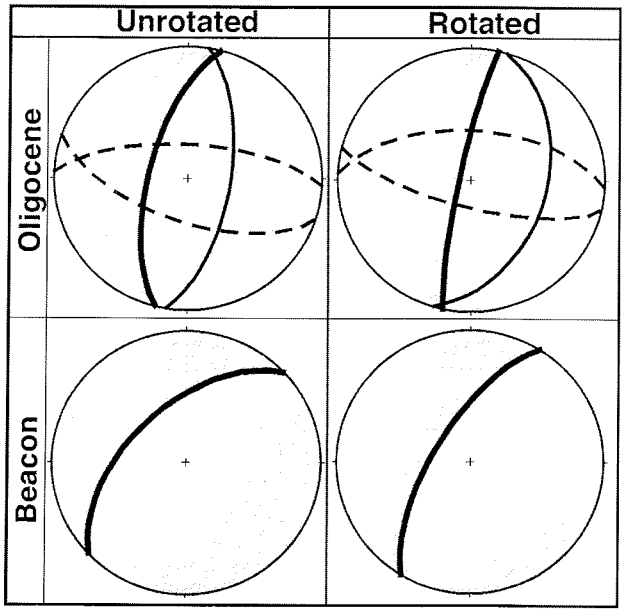

Fig. 16 - Stereoplots show average attitude of planes in Oligocene strata above 790 mbsf (upper) and in Beacon between 823-901 mbsf (lower), with *in situ* coordinates (left) and after rotation to restore average bedding to horizontal (right). Note the clearly defined conjugate fault pattern in the Oligocene strata becomes distorted by the rotation, suggesting the faulting post-dated stratal tilting. In contrast, the strongly dominant northeast-striking fracture set in the Beacon attains a 'typical' normal fault dip that is subparallel to the *in situ* Oligocene normal fault attitude after rotation, suggesting these faults may have formed prior to stratal tilting.

NE-striking faults may have formed prior to tilting of the sequence, implying an Early Oligocene or older age. Rotation of the steep microfaults and the clastic dykes in the 'shear zone', 790-804 mbsf, also points to their formation prior to stratal tilting (Figs. 5 & 6). The pre-tilt orientation of the Beacon fracture set is nearly identical in dip to the faults in the Oligocene strata, though the strike remains ~15 degrees more easterly. This suggests that faulting of about the same orientation continued in later Early Oligocene and Late Oligocene times. Possibly the oblique shear on the fractures below the shear zone (790-804 mbsf) and in the Beacon occurred in this period, because they had been rotated out of optimum orientation for continued dip-slip motion by the stratal tilting.

INDUCED FRACTURES IN CRP-3 CORE

PETAL, PETAL-CENTRELINE AND CORE-EDGE FRACTURES

Petal, petal-centreline and core-edge fractures are curviplanar drilling-induced fractures that form in the host rock below the drill bit (Lorenz et al., 1990; Li & Schmitt, 1997, 1998). A population of ~60 petal-centreline and core-edge fractures is present in CRP-3 core, mainly in the upper 225 m where the material is less indurated. This is a significantly smaller population of these induced fractures than in CRP-2A (Wilson & Paulsen, 2000). The reduced number may be due to the lower drilling-mud density used in CRP-3 compared to CRP-2, lowering the hydrostatic head exerted on the rock below, to the more indurated, stronger rock drilled in CRP-3, or to a combination of these factors.

Only a relatively small subset of the petal-centreline and core-edge fractures is in intact intervals that have been orientated. These form a well-defined group with an average north-northeast strike (Fig. 17). This orientation is *c.* 20° different than the average orientation of the same fracture types in the walls of the CRP-3 drill hole (Jarrard et al., this volume). The cause of this discrepancy is currently unknown.

LOW-ANGLE TENSILE FRACTURES

A large population of subhorizontal fractures is present in CRP-3 core. In fine-grained mudstones and siltstones, well-developed surface fractographic features including hackle plume, arrest lines and twist hackle are present on these fracture surfaces, clearly documenting their formation as Mode I extension fractures. In the abundant sandstones cored in CRP-3, surface features were rare on the subhorizontal fractures, but many are also likely Mode I extension fractures. There are a variety of mechanisms for causing axial tension in the core. For example, Mode I extension fractures are typically induced at the end of a core run, when the drilling assembly is retracted from the bottom of the hole to break the cored rock from the uncored interval below. Other causes include

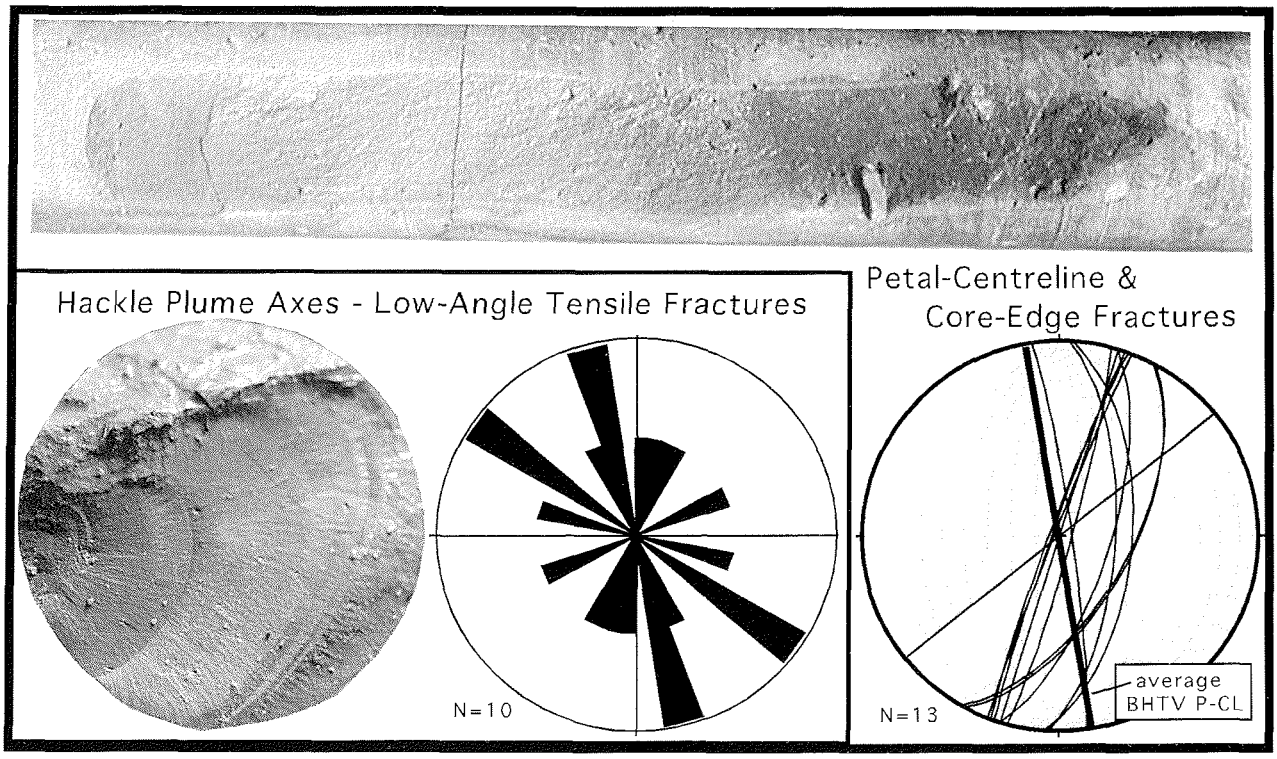

Fig. 17 - Drilling- and coring-induced petal-centreline and low-angle tensile fractures in CRP-3 core. Rose diagram showing hackle-plume axes on subhorizontal tensile fractures in oriented core (5 degree bins). Equal area stereoplot showing strike and dip of petal-centreline and core-edge fractures in core and the average petal-centreline strike interpreted from BHTV imagery. Core in photos is 45 mm in diameter.

raising the hydraulic chuck during drilling, handling-related flexure of the core, and disking, where tension arises when the core is released from the host rock upon entering the core barrel.

A small population of low-angle tensile fractures with hackle plume structures is present in orientated core. The hackle plume axes show a well-defined NNW trend (Fig. 17). Kulander and others (1990) have shown that, in the Appalachian Basin of eastern North America, propagation directions of these types of induced fractures, as mapped by the hackle plume trends, are controlled by the direction of maximum horizontal *in situ* stress in the host rock around the drill hole. The parallelism between the average trend of plume axes in CRP-3 core and the maximum horizontal stress direction defined by borehole breakouts in the drillhole walls demonstrates the same stress control of low-angle tensile fracture propagation at CRP-3.

SIGNIFICANCE OF CRP-3 FRACTURE PATTERNS

TIMING OF BRITTLE DEFORMATION

Microfaults in Oligocene strata of CRP-3 are intimately associated with injection of clastic dykes and with mineralization by diagenetic fluids. This shows that faulting was early, synchronous with dewatering and lithification of the strata, pointing to an Early Oligocene age. Our 'tilt test', however, suggests that microfaults in CRP-3 Oligocene strata above 790 mbsf formed after the major period of stratal tilting, which would imply a latest Oligocene or younger age. Bearing in mind, however, the very rapid sedimentation rates and short time interval spanned by the CRP-3 strata, these timing indicators are not inconsistent. Faulting may have post-dated deposition of most CRP-3 strata (between approximately 35-31 Ma), but commenced in the latest Early Oligocene or Late Oligocene prior to complete lithification of the sequence. Our documentation of brittle faulting of very cohesive sediment or fully lithified rock indicates faulting continued subsequent to deposition, lithification, and tilting, but we have no firm upper limit on fault age (Tab. 1).

The timing of faulting in the Devonian Beacon Supergroup strata and the Jurassic(?) igneous porphyry that intrudes it is more difficult to constrain definitively. One possibility is that the extensive faulting, brecciation and hydrothermal alteration of these units occurred in the Jurassic, approximately coeval with intrusion of the porphyry. Two factors argue against this. First, no similar extensive deformation is associated with Jurassic Ferrar Dolerite intrusions into Devonian Beacon strata in the adjacent Transantarctic Mountains. Second, it would be fortuitous for faults formed in a Jurassic event to be nearly identical in orientation as Oligocene rift-related faulting, as observed. Although we can not rule this possibility out with available data, we suggest that it is more likely that the deformation we observe is related to development of the Transantarctic Mountains Front zone. This fault zone must have accommodated *c.* 3000 m of down-to-the-east offset of the Beacon and Ferrar rocks and must have initiated by the latest Eocene – earliest Oligocene,

Tab. 1 - Summary description of CRP-3 core fractures.

Category	Fracture Types	Geometry	Interpreted Age
Brittle Fault Zones			
A: ~260 mbsf	Breccia; veins	NNE, W dip [probable]	<Early Oligocene
B: ~539 mbsf	Breccia; veins	ENE, N dip [probable]	<Early Oligocene
Shear Zone	A. Breccia Margins B. Clastic Dykes C. Striated Microfaults	A. NW,NE, scattered B. NNW, subvertical C. NW, NE & subparallel to 'average bedding'; oblique slip	A. Early Oligocene B. Early Oligocene C. ?Early Oligocene, Late Oligocene or younger
Natural Fractures – Oligocene Strata	A. Microfaults B. Veins (mainly calcite) C. Clastic Dykes	All types: **NNE**, NW, ENE conjugate sets; mainly normal-sense dip-slip shear	All types: late Early Oligocene – Late Oligocene or younger
Natural Fractures – Devonian Beacon Strata	A. Microfaults B. Filled Fractures (cataclastic faults?) C. Breccia Margins	A. NE, W dip; oblique slip B. NE, W dip C. NW, NE, scattered	All types: Early Oligocene? [Jurassic??]
Jurassic? Porphyry	Microfaults	ENE, N dip; oblique slip	Early Oligocene? [Jurassic??]
Drilling-Induced Fractures	A. Petal-Centreline B. Low-angle Tensile	A. NNE-NNW strike B. Plume axes: NNW	Both: Contemporary Stress Field

which is the age of the oldest sedimentary rocks resting on the unconformity with the Devonian Beacon 'basement' at Cape Roberts (CRST, 2000). Our 'tilt test' suggests that the faults cutting the Beacon formed prior to the main episode of stratal tilting, which occurred in late Early Oligocene-Late Oligocene times (Jarrard et al., this volume). This is consistent with an 'early' faulting episode of latest Eocene – Early Oligocene age affecting the Beacon strata. We suggest that this early episode records the major down-to-the-east displacement along the Transantarctic Mountains front that dropped the Beacon floor of the rift basin. The NNE-striking, W-dipping dominant fault set in CRP-3 core and mapped at Roberts Ridge is younger, according to our 'tilt test', and most likely formed as the hinge margin of the basin flexed in response to Late Oligocene and younger subsidence due to growth faulting on the eastern margin of the Victoria Land Basin. A key test to discriminate between the alternatives of Oligocene or Jurassic faulting of the Beacon strata is to establish whether or not there is any relationship between the extensive hydrothermal activity that affected the breccias and northeast-striking fractures in the Beacon strata and the migration of large volumes of diagenetic fluids along the northeast-striking fractures in the Oligocene strata above.

KINEMATIC HISTORY FROM NATURAL FRACTURE SETS

The conjugate geometry and normal-sense, mainly dip-slip displacement associated with the microfaults in the Oligocene strata down to the 'shear zone' at 790 mbsf, documents a vertical maximum principal stress during deformation. Below that depth, moderate- to low-angle slip lineations become common, indicating oblique shearing, although normal-sense displacement remains dominant. Because the oblique lineations occur on fault surfaces with both shallow and steep dips, it is likely that the oblique shear marks reactivation of existing fracture surfaces. Some rare cases of multiple striae on fault surfaces support this interpretation. This interpretation implies that oblique shear followed the dominant normal-sense dip-slip fault displacement.

The fracture record from the intervals of CRP-3 that are orientated does not indicate any change in natural fracture strike with respect to age of strata or depth in the core and, therefore, we can not assign an age to the north-northeast or northwest fracture sets we have documented (Table 1). This same geometric pattern persists stratigraphically upward through the CRP-2A strata of late Early Oligocene and Late Oligocene age (Wilson and Paulsen, 2000). Based on these results, it appears that the same strain regime persisted through the Oligocene. Because we have no firm constraint on the relative timing of conjugate fault arrays with different strikes, we can not determine whether these represent discrete deformation episodes or if their formation overlapped in time. The association of clastic dykes and mineralization with all of them suggests, however, that they can not be significantly different in age. If only the dominant north-northeast and west-northwest geometric sets are considered, one possible interpretation is that development of the fault sets overlapped in time, with the orientation of the two horizontal stresses remaining approximately constant, but the relative magnitudes switching (*cf.* Angelier et al., 1984). The strong development of the north-northeast striking fault array indicates that a north-northeast-trending maximum horizontal stress was the dominant regime. We note that this fault set is oblique to the overall north-northwest orientation of the Transantarctic Mountains Front zone, implying oblique, transtensional shear along this structural boundary. A very similar geometric pattern of Cenozoic faults was documented by Rosetti et al. (2000) along the Victoria Land coast *c.* 100 km north of Cape Roberts, indicating the regional significance of this structural array and associated transtensional deformation.

ORIENTATIONS OF NATURAL FRACTURE SETS WITH RESPECT TO REGIONAL STRUCTURE

As illustrated by Figure 18, there are some strong similarities as well as some differences between the average microfault orientations we have documented in the CRP-3 core and both seismically-mapped regional faults on Roberts Ridge (Hamilton et al., 1998, 2001) and mesoscale faults mapped in outcrops onshore in the adjacent Transantarctic Mountains (Wilson, 1995) and to the north along the Victoria Land coast (Rosetti et al., 2000). Wilson (1995) documented north-northeast-striking normal faults along the Transantarctic Mountains Front which are nearly identical to the dominant microfault trend in the CRP-3 core. North-northeast to northeast-trending faults also dominate the western flank of Roberts Ridge and are inferred to mark the west-dipping boundary faults of the Cape Roberts Rift Basin (Hamilton et al., 1998, 2001). It is likely that the dominant northeast-striking and west-dipping natural fractures in CRP-3 represent this regional fault set. According to our interpretation of core data, the north-northeast faults would have formed in earliest Oligocene through latest Oligocene times, and are possibly younger, consistent with interpretations of offsets on seismic reflection profiles (Salvini et al., 1997; Hamilton et al., 1998, 2001).

East-northeast striking normal faults, developed primarily in proximity to transverse structures segmenting the rift flank, are present in outcrop in the Transantarctic Mountains (Wilson, 1995) and have also been inferred in the vicinity of Cape Roberts from high-resolution aeromagnetic data (Bozzo et al.,

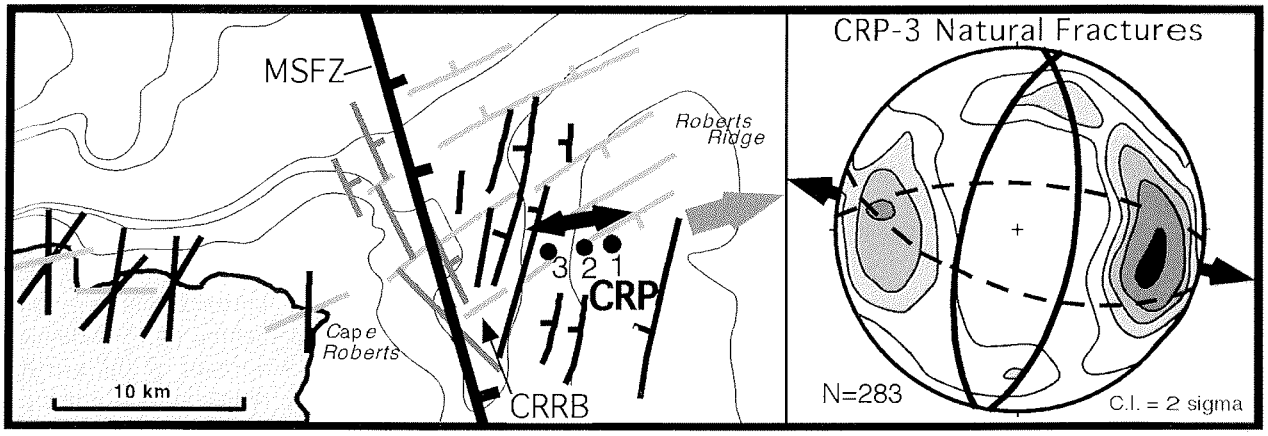

Fig. 18 - Orientation of natural fractures and *in situ* contemporary minimum horizontal stress directions with respect to offshore faults of the Cape Roberts Rift Basin (CRRB) and Roberts Ridge from Hamilton et al. (1998) and onshore mesoscale faults in Transantarctic Mountains outcrops from Wilson (1995); black lines are NNE faults; dark grey lines are NW faults; pale grey lines are ENE faults. Note that the dominant north-northeast natural fracture set in the core (stereoplot) is parallel to the dominant onshore fault set and to the fault array bordering the CRRB. The average transverse fault trend derived from core data is oblique to the east-northeast fault sets mapped onshore and across Roberts Ridge. The contemporary stress direction (black double arrow) is nearly perpendicular to the regional trend of the frontal fault zone of the Transantarctic Mountains, mapped by Hamilton et al. (2001) as the McMurdo Sound Fault Zone (MSFZ), whereas the natural fracture sets are oblique to this zone. The large grey arrow shows the average stratal dip from core, borehole and seismic data.

1997) and mapped across the Roberts Ridge area by Hamilton et al. (1998, in press). Within individual intact intervals of CRP-3, microfaults have east-northeast to east-west orientation but, on average throughout the core, have a west-northwest strike different from the onshore and Roberts Ridge fault patterns. The brittle fault zone at 539 mbsf, inferred to mark larger displacement, probably has an east-northeast orientation.

No faults parallel to the north-northwest trend of the Transantarctic Mountains were found onshore (Wilson, 1995). Hamilton et al. (1998, 2001) interpreted the main Transantarctic Mountains Front Zone offshore, termed by them the "McMurdo Sound Fault Zone", to have a northwest trend. They mapped northwest-trending faults along the western border of the Cape Roberts Rift Basin. Further north along the Transantarctic Mountains Front, Rosetti et al. (2000) found northwest-trending extensional and dextral strike-slip faults. Overall there is no well-developed, strongly orientated northwest-striking fault set in CRP-3 core, however northwest-striking faults are relatively common.

Though differing in some respects, in total the microfault pattern in CRP-3 core is strikingly similar to the orientations of previously mapped onshore and offshore faults in the region. Most significantly, a north-northeast fault set dominates the pattern, consistent with interpretations invoking Cenozoic dextral transtensional shear along the Transantarctic Mountains Front boundary (Wilson, 1992; 1995; Salvini et al., 1997; Rosetti et al., 2000). Our age data from CRP core indicates that this it likely to be of Early Oligocene and younger age. We note, however, that dextral transtension of Oligocene age is not consistent with the inferred north-northwest orientation of offshore growth faults implied by the east-northeast dips of fanning stratal sequences.

CONTEMPORARY STRESS DIRECTIONS

Borehole breakouts in the walls of the CRP-3 drillhole demonstrate that the present-day minimum horizontal stress direction is orientated east-northeast (Jarrard et al., this volume). This orientation is fully compatible with the large population of drilling-induced petal-centreline and core-edge fractures documented in CRP-2A core (Wilson and Paulsen, 2000), but is at a small oblique angle to the much smaller population of these induced fractures in CRP-3 core. The east-northeast minimum stress direction from CRP core and borehole data is oblique to the topographic slope of Roberts Ridge, and therefore we interpret it to record the *in situ* crustal stress direction in the Cape Roberts region. Based on considerations of frictional constraints and the types of induced fractures that occur within the CRP core and borehole walls, a strike-slip to normal-faulting crustal stress regime, in the sense of Anderson (1951), has been modeled (Moos et al., 2000; Jarrard et al., this volume). Modeling studies by Li and Schmitt (1998) indicate that the presence of both disc and petal-centreline fractures is compatible with either a normal faulting or strike-slip faulting stress regime, so our CRP core data is consistent with this interpretation.

The east-northeast orientation of the *in situ* minimum stress direction is approximately perpendicular to the regional trend of the Transantarctic Mountains Front structural boundary (Fig. 18). It is not compatible with the oblique stress orientations inferred from the natural fracture sets. One possible explanation for this is reorientation of

the minimum stress direction perpendicular to the regional Transantarctic Mountains topographic gradient post-dating Oligocene tectonism.

ACKNOWLEDGMENTS - This work was funded by NSF grant OPP-9527394 to T.J. Wilson. The drilling team and Alex Pyne deserve great credit for the successful coring operations. Our core fracture logging depended on the careful work of the CRP-3 core processors, Jo Anderson, Cliff Atkins, Nick Jackson and Matt Paterson. Shelley Judge carried out core scanning at the Drill Site Laboratory. Eric Plankell did the digital 'core stitching', and Shelley Judge compiled the core fracture data and helped with rotations and plotting of the fracture data; this project could not have been completed without their high-quality work. Cristina Millan made an inventory of CRP-3 microstructural features for her B.Sc. thesis. We thank Christian Buecker and Rich Jarrard for obtaining the orientated downhole logs used in our analysis. Rich Jarrard also completed much of the core orientation work that forms the basis of the orientation analysis we present here. DMT, Germany, provided reduced rates for lease of the CoreScan® for the Cape Roberts Project and Nodi Rafat donated his time to help with setup of the instrument at the Drill Site Laboratory. We thank Rick Allmendinger for providing stereonet programs used for our data analysis. Fabrizio Storti provided many useful comments that helped to improve this paper.

REFERENCES

Anderson E.M., 1951. *The Dynamics of Faulting*. Oliver & Boyd, Edinburgh, 206 p.

Angelier J., Colletta B. & Anderson R.E., 1984. Neogene palaeostress changes in the Basin and Range: A case study at Hoover Dam, Nevada-Arizona. *Geological Society of America Bulletin*, **96**, 347-361.

Barrett P.J., Henrys S., Bartek L.R., Brancolini G., Busetti M., Davey F.J., Hannah M.J. & Pyne A.R., 1995. Geology of the margin of the Victoria Land basin off Cape Roberts, southwest Ross Sea. In: Cooper A.K., Barker P.F. & Brancolini G. (eds.), *Geology and Seismic Stratigraphy of the Antarctic Margin, Antarctic Research Series*, **68**, AGU, Washington, 183-208.

Bozzo E., Ferraccioli F. & Wilson T., 1998. Structural Framework of a High Resolution Aeromagnetic Survey, Southwestern Ross Sea (Antarctica). *Terra Antartica*, **4**, 51-56.

Cape Roberts Science Team, 1998. Initial Report on CRP-1, Cape Roberts Project, Antarctica. *Terra Antarctica*, **5**, 1-187.

Cape Roberts Science Team, 1999. Studies from the Cape Roberts Project, Ross Sea, Antarctica. Initial Report on CRP2/2A. *Terra Antarctica*, **6**, 1-173.

Cape Roberts Science Team, 2000. Initial Report on CRP-3, Supplement, Cape Roberts Project, Antarctica, *Terra Antarctica*, **7**, 1-305.

Cooper A.K., Davey F.J. & Behrendt J.C., 1987. Seismic stratigraphy and structure of the Victoria Land Basin, western Ross Sea, Antarctica. In: Cooper A.K. & F.J. Davey (Editors), *The Antarctic Continental Margin: Geology and Geophysics of the Western Ross Sea* (Circum-Pacific Council Energy and Mineral Resources Earth Sci. Ser., 5B) Houston, TX, USA, 27-65.

Craw D. & Findlay R.H., 1984. Hydrothermal alteration of Lower Ordovician granitoids and Devonian Beacon Sandstone at Taylor Glacier, McMurdo Sound, Antarctica. *New Zealand Journal of Geology & Geophysics*, **27**, 465-475.

Ehrmann W.U., 2001. Variations in smectite content and crystallinity in sediments from CRP-3, Victoria Land Basin, Antarctica. This volume.

Elliot D.H., 1998. Ferrar phreatomagmatism; precursor to flood basalt eruption in Antarctica. *Journal of African Earth Sciences*, **27**, 65-66.

Fitzgerald P.G., 1992. The Transantarctic Mountains of southern Victoria Land: The application of apatite fission track analysis to a rift shoulder uplift. *Tectonics*, **11**, 634-662.

Fitzgerald P.G., 2001. Apatite fission track ages associated with the altered igneous intrusive in Beacon sandstone near the base of CRP-3, Victoria Land Basin, Antarctica. This volume

Grapes R.H., Reid D.L. & McPherson J.G., 1974. Shallow dolerite intrusion and phreatic eruption in the Allan Hills region, Antarctica. *New Zealand Journal of Geology and Geophysics*, **17**, 563-577.

Hamilton R.J., Sorlien C.C., Luyendyk B.P., Bartek L.R. & Henrys S.A., 1998. Tectonic regimes and structural trends off Cape Roberts, Antarctica. *Terra Antarctica*, **5**, 261-272.

Hamilton R.J., Luyendyk B.P., Sorlien C.C. & Bartek L.R., 2001. Cenozoic tectonics of the Cape Roberts Rift Basin and Transantarctic Mountains Front, Southwestern Ross Sea, Antarctica. *Tectonics*, **20**, 325-342.

Henrys S. A., Bücker C., Niessen F. & Bartek L. R., 2001. Correlation of seismic reflectors with the CRP-3 drillhole, Victoria Land Basin, Antarctica. This volume.

Jarrard R.D., Paulsen T. & Wilson T., 2001. Orientation of CRP-3 core, Victoria Land Basin, Antarctica. This volume.

Jarrard R.D., Bücker C., Wilson T. & Paulsen T., 2001. Bedding dips from the CRP-3 drillhole, Victoria Land Basin, Antarctica. This volume.

Jarrard R.D., Moos D., Wilson T., Bücker C. & Paulsen T., 2001. Stress patterns observed by borehole televiewer logging of the CRP-3 drillhole, Victoria Land Basin, Antarctica. This volume.

Korsch R.J., 1984. The structure of Shapeless Mountain, Antarctica, and its relation to Jurassic igneous activity. *New Zealand Journal of Geology and Geophysics*, **27**, 487-504.

Kulander B.R., Dean S.L. & Ward B.J. Jr., 1990. *Fractured Core Analysis: Interpretation, Logging, and Use of Natural and Induced Fractures in Core*. American Association of Petroleum Geologists Methods in Exploration Series, No. 8, 88 p.

Li Y. & Schmitt D.R., 1997. Well-bore bottom stress concentration and induced core fractures. *American Association of Petroleum Geologists Bulletin*, **81**, 1909-1925.

Li Y. & Schmitt D.R., 1998. Drilling-induced core fractures and in situ stress. *Journal of Geophysical Research*, **103**, 5225-5239.

Lorenz J.C., Finley S.J. & Warpinski N.R., 1990. Significance of coring-induced fractures in Mesaverde core, northwestern Colorado. *American Association of Petroleum Geologists Bulletin*, **74**, 1017-1029.

Millan C. 2001. Analysis of Microstructures in Core from the Victoria Land Basin, Antarctica. The Ohio State University, Columbus, B.Sc. Thesis.

Millan C., Wilson T. & Paulsen T., 2000. Microstructural analysis of faults and veins in core from the Victoria Land rift basin, Antarctica, GSA Abstracts with Program, Annual Meeting.

Moore J.C., Roeske S., Lundberg N., Schoonmaker J., Cowan D.S., Gonzales E. & Lucas S.E., 1986. Scaly fabrics from Deep Sea Drilling Project cores from forearcs, In: Moore, J.C., ed., *Structural Fabrics in Deep Sea Drilling Project Cores From Forearcs*, Geological Society of America, Memoir **166**, 55-74.

Moos D., Jarrard R.D., Paulsen T., Scholz E. & Wilson T., 2000. Acoustic Borehole Televiewer (BHTV) Results from CRP-2/2A, Victoria Land Basin, Antarctica. *Terra Antartica*, **7**, 279-286.

Morrison, A.D., 1989. Geological observations from Terra Cotta Mountain, upper Taylor Glacier. *New Zealand Antarctic Record*, **9**, 31-43.

Passchier S., 2000. Soft-sediment deformation features in Core from CRP-2/2A, Victoria Land Basin, Antarctica. *Terra Antartica*, **7**, 401-412.

Paulsen T., Wilson T., Moos D., Jarrard R. & Wilson G., 2000. Orientation of CRP2A core. *Terra Antartica*, **7**, 271-278.

Pompilio M., Armienti P. & Tamponi M., 2001. Petrography, mineral composition and geochemistry of volcanic clasts and the magmatic body of CRP-3, Victoria Land Basin, Antarctica. This volume.

Pyne, A.R., 1984. Geology of the Mt. Fleming area, South Victoria Land, Antarctica. *New Zealand Journal of Geology and Geophysics*, **27**, 505-512.

Rosetti F., Storti F. & Salvini F., 2000. Cenozoic noncoaxial transtension along the western shoulder of the Ross Sea, Antarctica, and the emplacement of McMurdo dyke arrays. *Terra Nova*, **12**, 60-66.

Salvini F., Brancolini G., Busetti M., Storti F., Mazzarini F. & Coren F., 1997. Cenozoic geodynamics of the Ross Sea region, Antarctica: Crustal extension, intraplate strike-slip faulting, and tectonic inheritance. *J. Geophys. Res.*, **102**, 24,669-24,696.

Setti M., Marinoni L. & Lopez-Galindo A., 2001. Crystal-chemistry of the smectites in the sediments of the CRP-3 drillcore, Victoria Land Basin, Antarctica:preliminary results. This volume.

Tessensohn F. & Wörner G., 1991. The Ross Sea rift system, Antarctica: structure, evolution and analogues. In: Thomson M.R.A., Crame J.A. & Thomson, J.W. (eds.), *Geological Evolution of Antarctica*. Cambridge University Press, New York, 273-277.

Van der Meer J.J.M., 2000. Microscopic Observations on the Upper 300 of CRP-2/2A, Victoria Land Basin, Antarctica. *Terra Antartica*, **7**, 339-348.

Wilson T.J., 1992. Mesozoic and Cenozoic kinematic evolution of the Transantarctic Mountains. In: Yoshida Y., Kaminuma K. & Shiraishi K. (eds.), *Recent Progress in Antarctic Earth Science*, Terra Sci., Tokyo, 303-314.

Wilson, T.J., 1993. Jurassic faulting and magmatism in the Transantarctic Mountains: Implications for Gondwana breakup. In: Findlay, R.H., Unrug, R., Banks, M.R., & Veevers, J.J. (eds)., *Gondwana 8: Assembly, Evolution and Dispersal*. Balkema, Rotterdam, 563-572.

Wilson T.J., 1995. Cenozoic transtension along the Transantarctic Mountains-West Antarctic rift boundary, southern Victoria Land, Antarctica. *Tectonics*, **14**, 531-545.

Wilson T.J., 1999. Cenozoic structural segmentation of the Transantarctic Mountains rift flank in southern Victoria Land, Antarctica. In: van der Wateren, F.M. and Cloetingh, S. (Editors), Lithosphere Dynamics and Environmental Change of the Cenozoic West Antarctic Rift System, *Global and Planetary Change*, **23**, 105-127.

Wilson T.J. & Paulsen T., 2000. Brittle Deformation Patterns of CRP-2/2A, Victoria Land Basin, Antarctica. *Terra Antartica*, **7**, 287-298.

Wise W., Smellie J.L., Aghib F.S., Jarrard R. & Krissek L.A., 2001. Authigenic smectite clay coats in CRP-3 drillcore, Victoria Land Basin, Antarctica, as a possible indicator of fluid flow: a progress report. This volume.